

3. EXPLANATORY NOTES¹

Shipboard Scientific Party²

INTRODUCTION

This chapter is designed to document the primary procedures and methods employed by the various shipboard laboratories to understand the basis for our preliminary interpretations. Shore-based methods used in subsequent work by various investigators should be explained in the publications produced by them.

Site Chapter Authorship

Descriptions of individual drilling sites, summaries of operations, and preliminary results and interpretations are contained in site chapters. This entire volume should be treated as a publication to which all scientists listed at the front of this volume contributed. The individual sections of site chapters were written by the following shipboard scientists listed in alphabetical order with no seniority implied:

Principal Results: Shipboard Scientific Party
Background and Objectives: Feary, Hine
Operations: Malone, Pollard
Lithostratigraphy: Andres, Betzler, Brooks, James, Machiyama,
Matsuda, Simo, Surlyk
Biostratigraphy: Brunner, Holbourn, Ladner, Li, Shafik
Paleomagnetism: Fuller, Molina Garza
Composite Depths: Mallinson
Organic Geochemistry: Mitterer
Inorganic Geochemistry: Swart, Wortmann
Physical Properties: Isern, Mallinson, Robin, Russell, Smart
Downhole Measurements: Huuse, Isern, Spence
Seismic Stratigraphy: Feary

¹Examples of how to reference the whole or part of this volume.

²Shipboard Scientific Party addresses.

Drilling Operations

Drilling sites are numbered consecutively from the first site drilled by the *Glomar Challenger* in 1968. Procedures for drilling multiple holes at one site involve removing the drill pipe from the seafloor, moving the ship a short distance, and then drilling a new hole. Multiple holes at one site are identified as A, B, C, and so on (e.g., 1126A, 1126B, 1126C, etc.).

Three coring systems were used during Leg 182: (1) advanced hydraulic piston corer (APC), (2) extended core barrel (XCB), and (3) rotary core barrel (RCB). The system type, the duration, and the rationale employed were designed to maximize core recovery and penetration rate; the details are explained in the "Operations" sections of each site chapter.

Drilled intervals are referred to in meters below rig floor (mbrf) measured from the kelly bushing on the rig floor to the bottom of the drill pipe. Meters below seafloor (mbsf) are calculated using the kelly bushing minus a sea-level correction factor. The mbrf depth of the seafloor is determined with a mudline core. Water depth is calculated by subtracting the distance from the rig floor height above sea level (determined at each site) from the drill-pipe mudline measurement in mbrf. This water depth typically differs from precision depth recorder measurements by one to several meters. The mbsf depths of core tops are calculated by subtracting the seafloor depth in mbrf from the core-top depth in mbrf. The core-top datums from the driller are the ultimate depth reference for any further depth calculation procedures.

For Leg 182 multiple APC holes were cored at each site, where possible, to construct a continuous composite section. This produces a meters composite depth (mcd) scale for each site, using interhole correlation to accommodate drilling gaps and/or core expansion (see "[Composite Depths](#)," p. 14).

Cores are taken in 9.5-m intervals. These intervals are cut into 1.5-m sections and are contained in a plastic liner with a 6.6-cm inside diameter. If recovery is less than 100% (as is frequently the case) and there are empty spaces in the core liner, the top of the core material in the 9.5-m interval obtained is equated with the top of the first section.

Curatorial and Core-Handling Procedures

Samples are identified with a curatorial code consisting of leg, site, hole, core number, core type, section number, and interval in centimeters measured from the top of the section. For example, 182-1126A-10H-1, 10–12 cm, would mean Leg 182, Hole 1126A at Site 1126, Core 10 (H indicating APC), Section 1, with the sample taken 10–12 cm down from the top of Section 1.

As soon as a core is retrieved on deck a sample is taken from the core catcher and taken to the paleontological laboratory for an initial age assessment. The core liner with the core inside is marked into section lengths. Each section length is labeled and the core is cut as marked. If whole-round samples are taken, the desired interval is identified and cut out of the core. When possible, whole-round samples are taken from the bottom of sections. During Leg 182 whole-round samples were taken for interstitial water (IW) analyses. For safety monitoring, small (~5 cm³) plugs of sediment are taken from the end of one section per core for headspace gas analysis. If pockets of gas are present a vacuum gas sample is taken through the core liner.

Each section is then sealed at the top and bottom by using acetone to glue color-coded plastic caps to the plastic core liner. A blue end cap marks the top of a section, a clear one marks the bottom, and a yellow cap marks the end of a section from which a whole-round sample has been removed; the sample code (e.g., IW) is written on any yellow cap used. The core sections are then carried into the laboratory and the lengths of the core sections and any samples taken are logged into the shipboard database.

After the core sections equilibrate to ambient laboratory temperature (~3 hr), they are run through the whole-core multisensor track (MST), and thermal conductivity measurements are made for soft sediment (see **“Physical Properties,”** p. 19). Cores are subsequently split lengthwise into working and archive halves. The archive half is used for nondestructive measurements: visual core description (VCD), paleomagnetism, magnetic susceptibility (MS), and color reflectance. Samples are taken from the working half for shipboard physical properties measurements (see **“Physical Properties,”** p. 19) before being sampled for additional shipboard and postcruise studies. The archive halves are photographed a whole core at a time, and close-up photographs are taken as requested. Finally, the core sections are put into labeled plastic tubes, sealed, and transferred to cold storage space aboard the drilling vessel. Following Leg 182 all cores were transported in refrigerated containers to the Gulf Coast Repository of the Ocean Drilling Program in College Station, Texas.

LITHOSTRATIGRAPHY

Sediment Core Description Forms

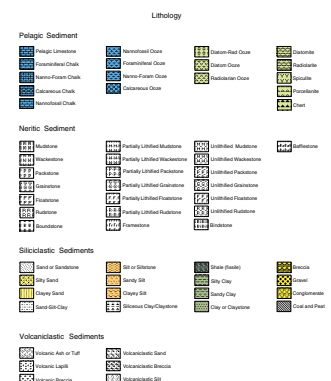
The sediment core description forms, or barrel sheets, summarize data obtained during shipboard analysis of each core (see the **“Core Descriptions”** contents list). The Ocean Drilling Program (ODP) conventions used for the compilation of each part of the core description forms and the exceptions to these procedures adopted by the Leg 182 Shipboard Scientific Party are described below.

Graphic Lithology Column

A modified version of the lithologic classification of Mazzullo et al. (1988) was used during Leg 182. The classification adopted here is outlined in **“Rock Classification and Principal Names,”** p. 6. Sediment type is represented graphically on the core description forms using the symbols illustrated in Figure F1.

In the **“Graphic Lithology”** column a maximum of three different lithologies (for interbedded sediments) or three different components (for mixed sediments) can be represented within the same core interval. Percentages are rounded to the nearest 10%, and only lithologies that constitute at least 10% of each core are shown. Minor lithologies that are present as thin interbeds within the major lithology are shown by a dashed vertical line dividing the lithologies. Components that are present as minor fractions of the main lithology are shown by a continuous vertical line. Grain size of siliciclastic sediments or texture of neritic carbonates (see **“Siliciclastic Sediments and Rocks,”** p. 8, and **“Neritic Calcareous Sediments and Rocks,”** p. 8) is shown in the col-

F1. Core description forms symbol key, p. 40.



umn to the left of the graphic lithology. However, note that only the mudstone and grainstone classes are displayed in Figure F1.

Bioturbation

Five degrees of bioturbation were differentiated (Fig. F1), similar to that of Droser and Bottjer (1986). The relative degrees of bioturbation are illustrated in the color-banded bioturbation column of the barrel sheets.

Sedimentary Structures

The location and nature of sedimentary structures are shown in the "Structure" column of the core description form. The symbols used to designate structures found in Leg 182 cores are shown in Figure F1.

Fossils and Ichnofossils

These columns indicate the occurrence of ichnofossil genera and major groups of macro- and microfossils. Bryozoans were classified using the growth-form scheme of Bone and James (1993). Symbols shown in this column are described in Figure F1.

Lithologic Accessories

This column indicates the position of secondary, diagenetic features such as ferruginous concretions or concretions in general. Symbols shown in this column are described in Figure F1.

Core Disturbance

Observations of drilling-related disturbance over an interval of 20 cm or more were recorded in the "Disturbance" column using the symbols shown in Figure F1. The degree of drilling disturbance in soft and firm sediments is as follows:

1. Slightly disturbed: bedding contacts are slightly deformed;
2. Moderately disturbed: bedding contacts have undergone extreme bowing;
3. Very disturbed: bedding is completely deformed as flowing, coring/drilling slough, and other soft sediment stretching and/or compressional shearing structures attributed to the coring/drilling; and
4. Soupy: intervals are water-saturated and have lost all aspects of original bedding.

The degree of fracturing in indurated sediments and rocks is described using the following categories:

1. Slightly fractured: core pieces are in place and broken;
2. Moderately fractured: core pieces are in place or partly displaced, and original orientation is preserved or recognizable (drilling slurry may surround fragments, i.e., drilling/coring "biscuits" are evident);
3. Highly fragmented: core pieces are probably in correct stratigraphic sequence (although they may not represent the entire sequence), but original orientation is lost; and

4. Drilling breccia: the core is crushed and broken into many small and angular pieces, with original orientation and stratigraphic position lost; often drilling breccia is completely mixed with drilling slurry.

Samples

The positions of samples taken from each core for analysis are indicated in the "Sample" column of the core description form as follows: SS (smear slide), THS (thin section), PAL (micropaleontology), and IW (interstitial water).

Color

After the core was split color was determined visually using the color chart of the Munsell Color Company (1994). In addition, color was measured with a Minolta CM-2002 spectrophotometer mounted on the archive multisensor track. These measurements were determined on the damp core surface, and Glad brand clear plastic film was used to cover the core. The Minolta CM-2002 measures reflected visible light in thirty-one 10-nm-wide bands ranging from 400 to 700 nm. Colors determined by this method correspond to those of the Munsell Color Company (1994). Routine measurements were made at evenly spaced intervals within each section, taking into account section length and the position of voids within the section.

Before and after obtaining measurements from each core, the spectrophotometer was calibrated for white color reflectance by attaching its white calibration cap. In addition, instrument calibration was checked using a white barium sulfate plate, which is the standard used for calibrating laboratory-grade spectrophotometers. These white color calibrations were made to avoid variation in color readings due to the laboratory environment (temperature, humidity, and background light) and instrument variations.

Note: After the cruise it was determined that a correction was applied erroneously to the color data by the recording software. The correction factors were not saved. Therefore, the absolute values of the raw data are incorrect. Calculation of color parameters such as L^* , a^* , and b^* will contain large errors. However, relative variations with depth are probably consistent. Relative spectral analysis (e.g., reflectance ratios, first derivative) can probably be performed with insignificant errors.

Lithologic Description

Core description forms consist of a list of major lithologies followed by a more detailed description of the composition (as determined from smear slides), color, sedimentary structures, and other notable features. Descriptions and locations of thin, interbedded, or minor lithologies are also included in the text. The terminology for the thickness of sedimentary beds and laminae follows McKee and Weir (1953): very thick bedded (>100 cm), thick bedded (30–100 cm), medium bedded (10–30 cm), thin bedded (3–10 cm), thickly laminated (>0.3 cm), and thinly laminated (<0.3 cm). The term "wispy lamination" was used to describe laminae with undulatory and anastomosing shapes.

Smear Slides and Thin Sections

Tables summarizing data from smear-slide and thin-section analyses (see the “[Core Descriptions](#)” contents list) include information about the sample location, whether the sample represents a dominant (D) or a minor (M) lithology in the core, and an estimate of sand, silt, and clay, together with all identified components. The following categories were used: trace (<0.1%), rare (0.1%–1%), present (1%–5%), common (5%–20%), abundant (20%–50%), and dominant (>50%).

Sediment and Rock Classification

Grain Types and Classifications

Grain types in granular sediments and rocks were classified according to mineralogy: (1) pelagic calcareous and siliceous, (2) neritic calcareous and siliceous, and (3) siliciclastic particles. Their definitions are as follows:

1. Pelagic grains are fine-grained skeletal debris produced within the upper part of the water column in open-marine environments by (a) calcareous microfauna and microflora (foraminifers, pteropods, nannofossils, and associated organisms) and (b) siliceous microfauna and microflora (radiolarians, diatoms, and associated organisms).
2. Neritic grains are coarse- to fine-grained particles and consist of calcareous and siliceous skeletal and nonskeletal grains and fragments (e.g., bioclasts, peloids, and micrite). Note that the term micrite is used to define very fine calcareous particles (<4 μm) of indeterminate origin.
3. Siliciclastic grains are (a) grains comprising minerals and rock fragments that were eroded from plutonic, sedimentary, and metamorphic rocks; and (b) grains comprising glass shards, rock fragments, and mineral crystals that were produced by volcanic processes.

Pelagic carbonates contain more than 50% pelagic grains, whereas neritic carbonates contain more than 50% neritic grains. Siliciclastic sediments and rocks are composed of more than 50% siliciclastic grains.

Rock Classification and Principal Names

Sediments and rocks were named on the basis of composition and texture using a principal name together with major and minor modifiers (Table [T1](#)). Principal names define the degree of consolidation (firmness) and granular sediment class. Composition is the most important classifier for pelagic and siliciclastic sediments and rocks, whereas texture is significant for the classification of neritic calcareous sediments and rocks (Table [T2](#)). Composition and texture of cored sediments and rocks were determined aboard ship by visual observation and visual estimates in smear slides, thin sections, and coarse fractions. Calcium carbonate content was qualitatively estimated in smear slides and quantitatively estimated by coulometric analysis (see “[Organic Geochemistry](#),” p. 16).

T1. Lithologic description of granular sediments and rocks, [p. 58](#).

T2. Lithologic description of non-pelagic calcareous sediments and rocks, [p. 59](#).

Firmness

Firmness of recovered materials was defined as in Gealy et al. (1971). Three classes of firmness were used to describe calcareous sediments and rocks:

1. Unlithified: soft sediments that have little strength and are readily deformed under the pressure of a fingernail or the broad blade of a spatula. This corresponds to the term “ooze” for pelagic calcareous sediments. In neritic calcareous sediments the prefix “unlithified” is used (e.g., unlithified packstone).
2. Partially lithified: firm but friable sediments that can be scratched with a fingernail or the edge of a spatula blade. The term “chalk” is used for firm or friable pelagic calcareous material. In neritic calcareous sediment the prefix “partially lithified” is used (e.g., partially lithified grainstone).
3. Lithified: hard, nonfriable, cemented rock that is difficult or impossible to scratch with a fingernail or the edge of a spatula. The term “pelagic limestone” (lithified ooze) is used for pelagic calcareous material. In neritic calcareous material a modified Dunham (1962) classification scheme (see “[Neritic Calcareous Sediments and Rocks](#),” p. 8) is used.

Two classes of firmness were used to describe siliceous sediments and rocks:

1. Soft: sediment core can be split with a wire cutter. Soft terrigenous sediment, pelagic clay, and transitional calcareous sediments are termed sand, silt, or clay; and
2. Hard: the core is hard (i.e., consolidated or well indurated) if it must be cut with a hand or diamond saw. For these materials the suffix “-stone” is added to the soft-sediment name (e.g., sandstone, siltstone, and claystone). Note that this varies from terms used to describe neritic calcareous sediments for which the suffix -stone has no firmness implications.

For a better visualization of the different intensities of sediment lithification, degrees of firmness are also shown in the “Consolidation” column of the core descriptions (Fig. [F1](#)).

Pelagic Sediments and Rocks

Principal names used to describe pelagic sediments and rocks during Leg 182 are as follows:

1. Pelagic clay: unconsolidated authigenic pelagic material (>15%) and siliceous pelagic sediment (lithified examples are termed pelagic claystone);
2. Ooze: unconsolidated calcareous and/or siliceous pelagic sediment;
3. Chalk: firm pelagic sediment composed predominantly of calcareous pelagic grains;
4. Pelagic limestone: hard pelagic sediment composed predominantly of calcareous pelagic grains;

5. Radiolarite, diatomite, and spiculite: firm pelagic sediment composed predominantly of siliceous radiolarians, diatoms, and sponge spicules, respectively;
6. Porcellanite: a well-indurated rock with the texture, hardness, conchoidal fracture, and general appearance of unglazed porcelain (less hard, dense, and vitreous than chert); and
7. Chert: vitreous or lustrous, conchoidally fractured, highly indurated rock composed predominantly of authigenic silica.

Neritic Calcareous Sediments and Rocks

Neritic calcareous sediments and rocks were classified using a modification of the original Dunham (1962) classification, in conjunction with depositional textures described by Embry and Klovan (1971; Figure F2):

1. Mudstone: mud-supported fabric with less than 10% grains (grains <2 mm in size);
2. Wackestone: mud-supported fabric with greater than 10% grains (grains <2 mm in size);
3. Packstone: grain-supported fabric with intergranular mud (grains <2 mm in size);
4. Grainstone: grain-supported fabric with no mud (grains <2 mm in size);
5. Floatstone: matrix-supported fabric (grains >2 mm in size); and
6. Rudstone: grain-supported fabric (grains >2 mm in size).

Siliciclastic Sediments and Rocks

Texture, structure, and composition are the main criteria for the selection of a principal name for siliciclastic sediments and rocks. The Udden-Wentworth grain-size scale (Fig. F3; Wentworth, 1922) defines the grain-size ranges and the names of the textural groups (gravel, sand, silt, and clay) and subgroups (fine sand, coarse silt, etc.). This grain-size scale was also used in carbonate rocks. When two or more textural groups or subgroups are present, the principal names appear in order of increasing abundance. Eight major textural categories can be defined on the basis of the relative proportions of sand, silt, and clay (Fig. F4). Distinguishing between some size categories is difficult (e.g., silty clay and clayey silt) without accurate measurements of weight percentages. The terms conglomerate and breccia are the principal names of gravels with well-rounded and angular clasts, respectively.

Major and Minor Modifiers

To describe the lithology of the granular sediments and rocks in greater detail, the principal name of a granular sediment class is preceded by major modifiers and followed by minor modifiers (Table T1). Minor modifiers are preceded by the term “with.” The most common uses of major and minor modifiers are to describe the composition and textures of grain types that are present in major (25%–40%) and minor (10%–25%) proportions. In addition, major modifiers can be used to describe grain fabric, grain shape, and sediment color.

The composition of pelagic grains can be described in greater detail with the major and minor modifiers “nannofossil,” “foraminifer,” “calcareous,” and “siliceous.” The terms calcareous and siliceous are used to

F2. Classification of limestones according to depositional texture, p. 44.

Allochthonous carbonates original components not organically bound during deposition				Autochthonous limestones original components organically bound during deposition		
Less than 10% >2-mm components		Greater than 10% >2-mm components		Boudinable		
Contains lime mud (<0.05 mm)		No lime mud				
Mud supported		Grain supported		By irregularly shaped and/or flattened grains		
Less than 10% grains (>0.05 mm)		Greater than 10% grains		By angular to sub-angular grains		
				By angular to sub-angular grains in a rigid framework		
Mudstone	Wackestone	Packstone	Grainstone	Floatstone	Rudstone	Bedstone
				Bedstone	Bedstone	Framestone

F3. Grain-size classification of terrigenous sediments, p. 45.

Millimeter (mm)	International units	Phi (φ)	International size class
4750	—	—	Boulder
3000	—	-0.5	
2000	—	-1.0	Cobble
1500	—	-1.5	
1000	—	-2.0	Very coarse sand
750	—	-2.5	
500	—	-3.0	Coarse sand
375	—	-3.5	
250	—	-4.0	Medium sand
175	—	-4.5	
125	—	-5.0	Fine sand
90	—	-5.5	
63	—	-6.0	Very fine sand
45	—	-6.5	
30	—	-7.0	Silt
20	—	-7.5	
15	—	-8.0	Clay
10	—	-8.5	
7.5	—	-9.0	Very fine clay
5	—	-9.5	
3.75	—	-10.0	Fine clay
2.5	—	-10.5	
1.75	—	-11.0	Medium clay
1.25	—	-11.5	
0.875	—	-12.0	Coarse clay
0.6	—	-12.5	
0.425	—	-13.0	Very fine clay
0.25	—	-13.5	
0.15	—	-14.0	Clay
0.075	—	-14.5	

F4. Classification scheme used for siliciclastic sediments and rocks, p. 46.



and modified by Okada and Bukry, 1980) was also made, particularly where better biostratigraphic resolution was possible with the latter. The zonation of Martini (1971) represents a good framework for biostratigraphic discrimination of midlatitude floral assemblages. The Cenozoic zonal schemes of Martini (1971) and Okada and Bukry (1980), together with the geomagnetic polarity time scale, are presented in Figure F5. Proxies to some of the defining events of the (sub)zones of Martini (1971) and Okada and Bukry (1980) are used, following Shafik et al. (1998), and are included in Figure F6. Cenozoic biostratigraphic events, including but not limited to the zonal/subzonal indicators of Martini (1971) and their proxies, are listed in Table T3.

Methods

Standard smear slides were made of all soft lithologies. Smear slides of indurated lithologies were prepared using the technique of Monechi and Thierstein (1985). Calcareous nannofossils were examined by means of standard light microscope techniques under cross-polarized and transmitted light at 1000x. We have adopted a simple system to characterize preservational states:

- VG = very good (all specimens are in pristine condition and can be identified with certainty);
- G = good (little or no evidence of dissolution and/or secondary overgrowth of calcite; diagnostic characters fully preserved; all specimens can be identified);
- M = moderate (dissolution and/or secondary overgrowth; partially altered primary morphological characteristics; however, nearly all specimens can be identified at the species level); and
- P = poor (severe dissolution, fragmentation, and/or secondary overgrowth with primary features largely destroyed; many specimens cannot be identified at the species level and/or generic level).

Relative abundance estimates for individual species were categorized as below:

- D = dominant (>100 specimens of a species per field of view),
- A = abundant (10–100 specimens of a species per field of view),
- C = common (1–10 specimens per field of view),
- F = few (one specimen per 10 fields of view),
- R = rare (fewer than one specimen per 10 fields of view), and
- B = barren (no calcareous nannofossils found).

Planktonic Foraminifera

We applied the zonal schemes of Berggren et al. (1995a, 1995b) and Jenkins (1985, 1993) for the Cenozoic. Ages of species datum levels (Table T4) are largely from Berggren et al. (1995a, 1995b, and references therein) and augmented by ages from Chaproniere et al. (1995) in reference to the zonal marker species of Jenkins (1985, 1993) (Fig. F7). In some cases datum level ages were amended on the basis of shipboard magnetostratigraphy. Taxonomic concepts for Neogene and Paleogene taxa are illustrated in Kennett and Srinivasan (1983), Bolli and Saunders

F6. The zonal schemes of Martini (1971) and Bukry and Okada (1980), p. 51.

F7. The events that define the zonal scheme of Jenkins (1985, 1993), p. 52.

Age (Ma)	Zones	Datum Levels
(1)		
2.0	BN14 Gr. truncatuloidea	Globobulimina truncatuloidea
3.2	BN13 Gr. inflata	Globobulimina inflata
4.5	BN12 Gr. punctulata	Globobulimina pilosula
4.2	BN11 Gr. pilosula	Globobulimina punctulata
6.8	BN10 Gr. conomastota	Globobulimina conomastota
10.1	BN9 Gr. neogibberula	Neogibberulina continiosa
11.4	BN8 Gr. nympha	Neogibberulina nympha
12.1	BN7 P. mayeri	Paraglobobulimina mayeri
15.1	BN6 Gr. subulata	Orbulina subulata
16.3	BN5 Gr. gibberula	Pragobulimina gomozensis curva
18.8	BN4 Gr. woodi connecta	Globobuliminitalia woodi connecta
20.0	BN3 Gr. woodi woodi	Globobuliminitalia woodi woodi
23.2	BN2 Gr. delticata	Globobulimina delticata
28.5	BN1 T. angulata	Chitiglobulimina cubensis
30.0	BN0 Gr. angulata	Subbotina angulata
31.5	BN0 Gr. brevis	Subbotina brevis
33.4	BN0 Gr. subulata	Subbotina subulata
37.7	BN0 Gr. aculeata	Aculeolina aculeata
41.2	BN0 Gr. inflata	Chitiglobulimina cubensis
42.9	BN0 Gr. angulata	Globobulimina inflata
50.8	BN0 Gr. inflata	Microbulimina inflata
54.0	BN0 Gr. inflata	Microbulimina inflata
59.2	BN0 Gr. inflata	Pseudobulimina wilsonensis
60.0	BN0 Gr. inflata	Microbulimina inflata
59.2	BN0 Gr. inflata	Planorbina inflata pseudomartini
(84.5)	BN0 Gr. inflata	Globobulimina daubergensis
64.7	BN0 Gr. inflata	Globobulimina daubergensis

(1985), Toumarkine and Luterbacher (1985), Jenkins (1971), and Hornibrook et al. (1989).

Unlithified to semilithified core sediment samples were wet-sieved over a 63- μm mesh screen and dried. Lithified material was crushed to pea size, boiled in a solution of Calgon diluted to 1% by weight, and then sieved and dried as before. Planktonic species relative abundances were estimated qualitatively and reported using the following categories:

- D = dominant (>30%),
- A = abundant (10%–30%),
- F = few (5%–10%),
- R = rare (1%–5%),
- P = present (<1%), and
- B = barren (no planktonic foraminifers).

Preservational characteristics were determined as follows:

- VG = very good (no evidence of breakage or dissolution),
- G = good (>90% of specimens unbroken),
- M = moderate (30%–90% of the specimens unbroken), and
- P = poor (strongly recrystallized or dominated by fragments and broken or corroded specimens).

Benthic Foraminifers

Benthic foraminifers were examined from the >63- μm size fraction. However, in samples in which tests are strongly recrystallized only the >150- μm size fraction was studied. Initial processing of the core-catcher samples used for benthic and planktonic foraminiferal studies was similar. The generic classification of Loeblich and Tappan (1988) was used with some exceptions, which mainly reflect subsequent taxonomic revisions. Taxonomic assignments followed those of van Morkhoven et al. (1986), Miller and Katz (1987), Thomas (1990), Katz and Miller (1991), Mackensen and Berggren (1992), and Mackensen (1992).

Benthic foraminifers provide limited biostratigraphic age control for Leg 182 samples and all zones recognized are local assemblage zones. Benthic foraminifers are used to estimate paleobathymetry, to identify periods of downslope transport of platform-derived material, and to identify major changes in paleocirculation regimes. Paleobathymetric estimates are primarily based on van Morkhoven et al. (1986). Bathymetric zones are defined as follows:

- IN = inner neritic (0–30 m),
- MN = middle neritic (30–100 m),
- ON = outer neritic (100–200 m),
- UB = upper bathyal (200–600 m),
- MB = middle bathyal (600–1000 m),
- LB = lower bathyal (1000–2000 m),
- UA = upper abyssal (2000–3000 m), and
- LA = lower abyssal (>3000 m).

The relative abundances of benthic foraminifers were estimated as follows:

- A = abundant (>10% of the fauna),
- C = common (3%–10% of the fauna),
- F = few (1%–3% of the fauna),
- R = rare (<1% of the fauna), and
- B = barren.

Preservational characteristics were indicated as follows:

- VG = very good (no evidence of breakage or dissolution),
- G = good (>90% of specimens unbroken),
- M = moderate (30%–90% of the specimens unbroken), and
- P = poor (dominated by recrystallized tests or by fragments and broken or corroded specimens).

PALEOMAGNETISM

Paleomagnetic work during Leg 182 consisted of long-core measurements of the natural remanent magnetization (NRM) of archive-half core sections before and after alternating field (AF) demagnetization, as well as NRM measurements and progressive demagnetization of discrete samples collected from the working half of core sections.

Long-core remanence measurements and AF demagnetization were performed using a computer-interfaced, pass-through, cryogenic direct-current superconducting quantum interference device (DC-SQUID), magnetometer (2-G Enterprises Model 760-R), and an AF demagnetizer (2-G Enterprises Model 2G-600) capable of reaching peak inductions of 80 mT at 200 Hz. The background noise level of the magnetometer is on the order of 10^{-10} Am². The large volume of core material within the sensing region of the magnetometer, which is ~ 100 cm³, permits the measurement of cores with remanent intensities as weak as $\sim 10^{-5}$ A/m. The data acquisition program collects magnetic moment data in the cgs system (emu). Data were later reduced to produce moments in SI units, with intensities in amperes per meter calculated using the magnetometer volume response functions.

Because of concerns over the reliability of remanence measurements of weakly magnetized carbonate rocks, the noise level was estimated from repeated runs of empty trays and was found to lie within the range reported from other ODP legs (10^{-9} – 10^{-10} Am²). During transit the reliability of the measurements of the cryogenic magnetometer was further tested on discrete samples of washcore of a homogeneous mixture of carbonate mudstone. Cubic samples (~ 10 cm³) were given a horizontal anhysteretic remanence (ARM) diagonally across a cube face. The intensity of the ARM was progressively increased using inductions of 5 to 50 mT, resulting in magnetic moments per unit volume (intensity) ranging between $\sim 5 \times 10^{-5}$ and 2.5×10^{-3} A/m. Two measurements were made in the cryogenic magnetometer, with an inversion of the horizontal axes of the sample. The antipodality of the remanence in both orientations as well as the ratios of the horizontal components x and y were plotted vs. the intensity of the ARM. From this experiment it was concluded that antipodality of $>170^\circ$ was observed only when the sample intensity was $>2 \times 10^{-4}$ A/m. The ratios of the horizontal axes are near the expected unit value for intensities $>2 \times 10^{-4}$ A/m, although moments measured when the samples were oriented in archive coordinates (sample +X/+Y direction = sensor +X/+Y direction) were consistently

higher (by ~5%) than moments measured in working coordinates. There appears to be no simple explanation for this observation.

Archive halves of all core sections were measured, unless coring or drilling-related deformation was noted. The demagnetization sequence applied to each core section was often dictated by the flow of core through the core laboratory. A five-step demagnetization scheme consisting of NRM and AF demagnetization at 5, 10, 15, and 20 mT was used in the first material recovered, but was later reduced to two or three steps. In most cases peak inductions of 20 mT were sufficient to isolate a characteristic magnetization and determine magnetic polarity, ensuring that the archive halves remain useful for shore-based high-resolution studies of magnetic remanence. For data collection a 5-cm measurement interval with 10-cm headers and trailers was first selected, although it was later increased to 10 cm in high-sedimentation-rate intervals. The large leader and trailer distance was used to allow possible future deconvolution of the long-core data. Measurements within 10 cm of the ends of each section may be compromised by edge effects, with false apparent low intensities and inaccurate directions occurring where the response function of the SQUID sensors (12–15 cm) averages empty space with the core signal. Directional data were collected using ODP orientation conventions (the sample +X axis is oriented toward the double line inscribed on the core liner of the working half). Core orientation of APCs was achieved using a Tensor tool mounted on the core-barrel assembly. Core photographs were examined to delete remanence data from disturbed or missing intervals. For each site we produced a set of tables that contain the cleaned data. The raw data are available in the JANUS database.

Discrete samples were collected from working halves in standard ~7-cm³ plastic cubes with orientation marks on the bottom of the sampling cube pointing upcore. Intervals of coring- or drilling-related core deformation were avoided. The shipboard long-core cryogenic magnetometer was used to measure the NRM of the discrete samples. Samples were measured in a tray designed to hold a maximum of seven samples. Discrete samples were also used for rock magnetic experiments, including isothermal remanent magnetization (IRM) acquisition and AF demagnetization of the saturation IRM. An Analytical Services Company pulse magnetizer was used for this purpose.

Low-field MS was measured for all whole-core sections as part of the MST analysis (see **“Physical Properties,”** p. 19). The MST susceptibility meter (a Bartington Model MS-2 with an MS2C sensor; coil diameter = 88 mm, operating frequency = 0.565 kHz) has a nominal resolution of 2×10^{-6} SI. Susceptibility was determined at 8-cm intervals using a 10-s integration time. The “units” option was set on SI units, and the values were stored in the JANUS database in raw count units. To convert to SI volume susceptibilities (bulk), these values should be multiplied by a correction factor to account for the volume of material that passed through the susceptibility coils. The correction factor for a standard ODP core is ~0.66 (= 1/1.5). No correction was applied to any figures illustrating magnetic susceptibilities in the “Paleomagnetism” sections in this report. Magnetic susceptibility of discrete samples obtained from the working half was measured using a Bartington MS2 susceptibility meter with a dual frequency MS1B Sensor. Magnetic susceptibility was used as a first-order measure of the amount of ferrimagnetic material and as a correlation tool.

Where AF demagnetization successfully isolated the characteristic component of remanence, paleomagnetic inclinations were used to de-

fine polarity zones. The revised time scale of Cande and Kent (1995), as presented in Berggren et al. (1995b), was used as a reference for the ages of Cenozoic polarity chrons.

COMPOSITE DEPTHS

Introduction

Core recovery from a single hole is generally insufficient to obtain a complete geologic section. To maximize recovery of complete geologic sections during Leg 182, multiple holes were drilled at each site, where possible, with cores offset in depth by ~2–3 m. The offset depths and multiple holes ensured that most intervals missing within a single APC hole were recovered in an adjacent hole. The degree of continuity of the recovered section at each site was assessed by development of composite depth sections using the Splicer software, following the general methodology first used during Leg 138 (Hagelberg et al., 1992). Similar methods were used during Legs 154 (Curry, Shackleton, Richter, et al., 1995), 162 (Jansen, Raymo, Blum, et al., 1996), 167 (Lyle, Koizumi, Richter, et al., 1997), and 177 (Gersonde, Hodell, Blum, et al., 1999). This section describes the methods used to produce composite and spliced sections during Leg 182, using the Splicer software.

Data Acquisition

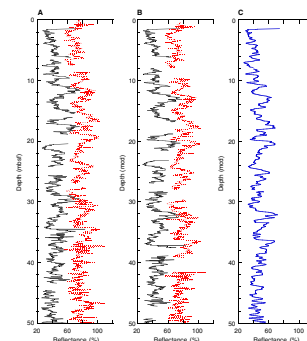
Cores recovered from each site were cut into 150-cm whole-round sections and allowed to equilibrate to ~20°C. Each core section was then analyzed for physical properties on a MST (see “**Physical Properties**,” p. 19). Split cores were analyzed using a color spectral reflectance scanner (see “**Lithostratigraphy**,” p. 3). Biostratigraphic data (first-appearance datum and last-appearance datum) from cores were also incorporated into the database for composite section development (see “**Biostratigraphy**,” p. 9).

Composite Section Development

The physical properties and biostratigraphic data described above were imported into the Splicer (version 2.0) software package. Splicer is an interactive, Unix-based software package designed by Peter DeMenocal and Ann Esmay at Lamont-Doherty Earth Observatory (LDEO) specifically for ODP stratigraphic correlation purposes. During composite section construction, data were culled to avoid the use of anomalous values resulting from voids and disturbed intervals in the cores. Natural gamma-ray emissions and color spectral reflectance data in the 400- and 700-nm bands provided the best lithologic parameters for correlation. Biostratigraphic data provided additional datums for correlation purposes, especially where correlations based on physical properties data were ambiguous.

The Splicer software allows for direct graphical and statistical comparison of data from each hole (Fig. F8). Tie lines are drawn between apparently correlative features present in the data (data excursions, peaks, troughs, and plateaus). The software provides a statistical analysis of the correlation over an adjustable depth range (typically ± 2 m). By convention, ODP sample and core depths were recorded as mbsf beginning at the top of the first core of a hole. Correlated features were then depth

F8. Color reflectance records from Holes 1126B and 1126C, p. 53.



aligned by linearly adjusting the data and ODP coring depths downward on a core-by-core basis. Correlations and alignments were continued downward for each core in each hole, using data from one hole to fill in data gaps in another hole. No depth adjustments (stretching or squeezing) were made to the data within a core. Correlation of events, involving alignment of data present in multiple holes, provided verification of the extent of recovery of the sedimentary section. Utilization of at least two different physical properties allowed hole-to-hole correlations to be made with greater confidence than would be possible with only a single parameter. Chronostratigraphic correlations were continuously verified using biostratigraphic information. The resulting adjusted depth scale is called the mcd, and the section produced by the aligned cores is termed a composite depth section. All adjustments to the data are written to a data output file (Table T5). The offset column allows conversion of sample depths from mbsf to mcd, effectively creating a sampling strategy guide. The mcd depth for any point within a core equals the mbsf depth plus the offset. A table is presented in each site chapter summarizing core offsets for conversion from mbsf to mcd scales.

Core distortions are typically caused by the drilling process. The offsets between mbsf and mcd scales result both from random uncertainty in mbsf depths as a result of ship motion and heave and from differential distortion of cores during the coring and retrieval process. For example, core expansion typically occurs at the tops of cores, whereas the sediment at the base of a core may be compressed. The expansion causes the composite section depths (mcd) to be greater than the mbsf depths, typically by ~10%. Because cores are offset in depth between holes, distortion of any specific mbsf interval is different in different holes. As a result, it is not possible to precisely align all features between holes. Tie points were chosen in an attempt to optimize the alignment and correlation of features in multiple holes. Where possible, tie points were chosen in the middle to lower portion of cores, where the record is likely to have been least disturbed by expansion. Where correlations were uncertain based on physical properties, input from biostratigraphic data was sought. Core photographs and VCDs were also a useful reference source for identifying potentially correlative lithologic features within cores. Where overlapping data from other holes were unavailable, causing data gaps in the total section, the depth adjustment applied was the cumulative offset from the overlying aligned cores.

The Splicer software allows the user to merge, or splice, the best data from the composite section to produce a single spliced record representing the complete geologic section at each site (Fig. F8). The spliced record is constructed by patching the intervals missing in a single hole with data from adjacent holes. This process provides a single representative record of the physical properties parameters (e.g., MS, spectral reflectance, or gamma-ray attenuation [GRA] bulk density) for the entire section, which is ideally suited to guide core sampling for high-resolution paleoceanographic studies.

Splice tie points were made between adjacent holes where visually obvious features are strongly correlated. The splice operation is depth constrained so that no further core offset is possible. Because of core expansion and/or compression, the total length of the spliced record depends on which intervals of core were selected to construct it. Each splice was constructed by beginning at the mud line at the top of the composite section and working downward. Core intervals were chosen

T5. Splicer data output file, p. 67.

for the splice in an effort to minimize the inclusion of disturbed data. As in the composite section construction, no compression or expansion of the data are possible. Adjustments to the composite or spliced sections, such as a linear compression of the mcd scale within individual core intervals, are required to align all features exactly (e.g., Hagelberg et al., 1995).

ORGANIC GEOCHEMISTRY

The shipboard organic geochemistry analyses for Leg 182 included (1) real-time monitoring of volatile hydrocarbons for safety and pollution prevention; (2) inorganic carbon (IC) analyses to determine calcium carbonate content; (3) elemental analyses of total carbon (TC) and nitrogen; and (4) preliminary characterization of organic matter by Rock-Eval pyrolysis. All methods and instruments used during Leg 182 are described below; further details are available in Emeis and Kvenvolden (1986).

Volatile Hydrocarbons

Concentrations of light hydrocarbon gases were monitored at intervals of one sample per core following the standard headspace sampling method described by Kvenvolden and McDonald (1986). Upon core retrieval a 5-cm³ sediment sample was collected and placed in a 21.5-cm³ glass serum vial that was sealed with a septum and metal crimp cap. For a consolidated or lithified sample, rock chips were placed in the vial and sealed. After heating to 60°C for 20 min, a 5-cm³ volume of headspace gas was extracted from the vial using a standard glass syringe. When gas pockets were observed, vacutainer samples were collected directly from the core while still in the core liner by penetrating the liner using a syringe connected to a penetration tool.

Constituents of the headspace and vacutainer gas samples were routinely analyzed using a Hewlett Packard 5890 II Plus gas chromatograph (GC) equipped with an 8 ft × 1/8 in stainless steel column packed with HaySep S (100–120 mesh) and a flame ionization detector (FID). Concentrations of methane, ethane, ethene, propane, and propene were obtained. The headspace syringe or vacutainer was directly connected to the GC with a 1.0-cm³ sample loop. The carrier gas was helium, and the GC oven was held at 90°C. Data were collected using a Hewlett-Packard 3365 Chemstation data handling program.

When high concentrations of C₂₊ hydrocarbon gases or of nonhydrocarbon gases such as H₂S or CO₂ were found, gas samples were analyzed using the natural gas analyzer (NGA). The NGA system consists of a Hewlett-Packard 5890 II Plus GC equipped with two different columns and detectors. Hydrocarbons from methane to hexane were analyzed using a 60 m × 0.32 mm DB-1 capillary column and FID. The GC oven was heated at 40°C for 10 min and then to 65°C at 10°C/min. Nonhydrocarbon gases were analyzed isothermally (150°C) using a sequence of packed columns, a 15-cm HaySep R column connected to a 1-m molecular sieve column and a 2-m Poropak T column, and detected using a thermal conductivity detector (TCD).

Inorganic Carbon

Three 5-cm³ sediment samples were routinely selected from each core for IC analysis. Inorganic carbon concentration was determined using a Coulometrics 5011 CO₂ coulometer. An ~10- to 15-mg sample of freeze-dried, ground sediment was weighed and reacted with 2 N HCl. The liberated CO₂ was titrated and the endpoint determined by a photodetector. Percentage of CaCO₃, expressed as weight percent calcium carbonate, was calculated from the IC content, assuming that all evolved CO₂ was derived from dissolution of CaCO₃, by the equation

$$\text{CaCO}_3 \text{ wt\%} = 8.33 \cdot (\text{inorganic carbon wt\%}).$$

No correction was made for the presence of other carbonate minerals.

Carbon, Nitrogen, and Sulfur Analyses

Total carbon, nitrogen, and sulfur concentrations were determined using a Carlo Erba 1500 CNS elemental analyzer. About 10 mg of freeze-dried ground sediment was weighed and combusted at 1000°C in a stream of oxygen. Nitrogen oxides were reduced to N₂, and the mixture of CO₂, N₂, and SO₂ gases was separated by gas chromatography followed by thermal conductivity detection. Organic carbon (TOC) concentration was calculated as the difference between TC and IC concentrations. Atomic C/N values were calculated from TOC and nitrogen concentrations.

Organic Matter Characterization and Maturity Determination

The organic matter in selected organic carbon-rich sediment samples was characterized by pyrolysis using a Delsi Rock-Eval II system. This method is based on a whole-rock pyrolysis technique designed to characterize the type and maturity of the organic matter and to estimate the petroleum potential of the sediments (Espitalié et al., 1986). The Rock-Eval system incorporates a temperature program that initially expels volatile hydrocarbons (S₁) as the sample is heated at 300°C for 3 min and then, as the temperature increases from 300° to 600°C at 25°C/min, releases the hydrocarbons (S₂) resulting from thermal cracking of kerogen. S₁ and S₂ hydrocarbons are measured and reported in milligrams per gram of dry sediment. The temperature at which the kerogen yields the maximum amount of hydrocarbons during the S₂ program provides T_{max}, a parameter used to assess the maturity of the organic matter. Between 300°C and 390°C of the pyrolysis program, CO₂ (S₃) is released from the organic matter, trapped, measured by TCD, and reported in milligrams per gram of dry sediment. Rock-Eval II parameters are used to characterize organic matter by calculation of the following indices: hydrogen index (HI = S₂/TOC × 100); oxygen index (OI = S₃/TOC × 100); and S₂/S₃. Rock-Eval data are generally unreliable for samples containing <0.5% TOC.

INORGANIC GEOCHEMISTRY

Interstitial Water Sampling and Chemistry

Shipboard IW analyses were performed on 5- to 15-cm-long whole-round sections that were cut immediately after core retrieval on deck. Details of the sampling resolution are described in the individual site chapters. After extrusion from the core liner the surface of each whole round was carefully scraped with a spatula to remove potential contamination. Interstitial waters were collected using a titanium squeezer modified after the standard stainless steel squeezer of Manheim and Sayles (1974). After loading the squeezer pore water was extruded through prewashed Whatman no. 1 filters fitted on a titanium screen by applying pressures as high as 40,000 lb (~4150 psi) using a hydraulic press.

Interstitial water was collected into acid-washed (10% HCl) 50-mL plastic syringes through 0.45- μm Gelman polysulfone disposable filters. Samples for shipboard work were stored in plastic vials before analysis.

Interstitial water samples were routinely analyzed for salinity of total dissolved solids using a Goldberg optical handheld refractometer (Reichert). The alkalinity was measured by Gran titration using a Metrohm pH electrode and autotitrator. The pH was measured on the National Bureau of Standards scale as part of the alkalinity titration. In situ electrode potential measurements were made before squeezing the whole round, using a glass combination electrode and a Metrohm portable pH meter. The electrode was calibrated against TRIS and BIS buffers to calculate pH on the free H^+ scale (Gieskes et al., 1991). The pH determined in this fashion (ppH) was more reliable than that obtained during the alkalinity titration because the algorithm employed for pH measurement before the start of the alkalinity titration is adversely affected by degassing before the alkalinity measurements.

Dissolved chloride was determined by titration using the method of Gieskes et al. (1991). Silica, phosphate, and ammonium were determined by spectrophotometric methods using a Milton Roy Spectronic 301 spectrophotometer (Gieskes et al., 1991). The standard deviations for the analyses are given in Table T6.

Concentrations of sodium, potassium, magnesium, calcium, chloride, and sulfate were analyzed by ion chromatography using a Dionex DX-120. Standard deviations are given in Table T6. Measurements of chloride using ion chromatography were systematically higher by ~3%–5% than those obtained by titration, hence only titration results are reported. As a result of the interference of H_2S with the analysis of Cl^- by titration, all samples showing high concentrations of H_2S were treated with 100 μl of 30% H_2O_2 five min before analysis (Shipboard Scientific Party, 1997).

Concentrations of iron, lithium, and strontium were quantified using flame atomic emission (AES) or absorption (AAS) spectrometry on a Varian Spectra AA-20. Iron was determined directly in the alkalinity titration residues. Air-acetylene (Fe, Li) and nitrous oxide acetylene (Sr) flames were utilized. Standards for all flame AAS/AES techniques were matched in matrix composition to the samples (Li, Sr) or prepared in synthetic seawater (Fe). A more detailed description of all methods and standards for all analyses used can be found in Gieskes et al. (1991). The 1- σ standard deviations were ~2% for lithium and ~3%–4% for strontium.

T6. Standard deviations for chemical analyses, p. 68.

X-Ray Diffraction

Mineralogy was determined on solid carbonate samples using X-ray diffraction (XRD). Quantitative XRD analyses were performed on bulk samples to determine the relative percentage of aragonite, calcite, quartz, and dolomite. Samples were run in batches of 20 and scanned from 25° to 35°, counting for 1.0 s at 0.02° 2θ steps. To overcome the limitations of using multicomponent standards, conversion from peak areas to mineral weight percent was accomplished using the H-factor method of Hooten and Giorgetta (1977), modified to use low-Mg calcite as the common internal standard. In this method the areas of the peaks of interest were obtained relative to the calcite peak and calibrated using calibration curves from a series of two-component standards. The final weight percent of each mineral was adjusted to the appropriate carbonate concentration measured on the same sample (see “Organic Geochemistry,” p. 16). Overall, the accuracy of the XRD analysis is within 5% actual weight percent with a standard deviation of 3%.

PHYSICAL PROPERTIES

Introduction

Physical properties were measured on unsplit cores and on undisturbed portions of split cores. The MST was used on whole cores for nondestructive measurements of wet bulk density, compressional wave velocity, MS, and natural gamma radiation. Thermal conductivity measurements were made only on unconsolidated whole cores with the exception of Site 1129, where data were collected on consolidated split cores. Undrained shear strength, index properties, and compressional wave velocity (V_p) were measured at discrete intervals on split cores, usually at a frequency of one per section. Figure F9 shows the sequence of physical properties measurements made during Leg 182, and Table T7 lists the average sampling intervals for each of the physical properties data sets collected.

Physical properties measurements on Leg 182 were used to obtain (1) high-resolution records for hole-to-hole correlation, construction of complete stratigraphic sequences, and downhole log calibration; (2) information related to sediment composition, diagenesis, and consolidation history to help constrain the location of unconformities, sediment fracturing, and fluid migration; and (3) data for the calculation of synthetic seismograms (i.e., compressional wave velocity and bulk density) and for the calculation of local heat flow (i.e., thermal conductivity).

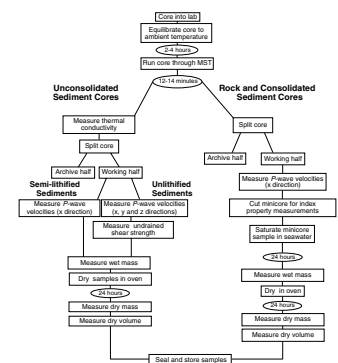
Shipboard Measurements

To ensure thermal homogeneity for all physical properties measurements, data were collected after equilibrating the cores to ambient room temperature (20°–25°C). Detailed information on the physical principles underlying the sampling methods discussed here can be found in Blum (1997).

Multisensor Track

The MST consists of an automated track that moves whole-core sections through sensors measuring MS, GRA bulk density, P -wave veloc-

F9. Physical properties measurements, p. 54.



T7. Sampling intervals for physical properties measurements, p. 69.

ity, and natural gamma radiation (NGR). Whole-round sections designated for shipboard geochemical analyses were removed before scanning.

MS, GRA, and NGR were measured on all cores regardless of collection method (i.e., APC, XCB, and RCB). *P*-wave velocities were measured only on APC-cored intervals because of the likelihood of discontinuous core, core disturbance, and/or a loss of coupling between the liner and the core with XCB and RCB drilling.

P-wave velocity (V_p) was measured at 4-cm intervals (4-s period) using a 500-kHz compressional wave pulse at a repetition rate of 1 kHz. The transmitting and receiving transducers are horizontally aligned perpendicular to the core axis. A pair of displacement transducers monitors the separation between the compressional wave transducers. Sediments must completely fill the liner for the *P*-wave logger to provide accurate results.

Magnetic susceptibility was measured using a Bartington Model MS-2 meter with an 80-mm internal diameter sensor loop (88-mm coil diameter), operating at a frequency of 565 Hz and an AF of 80 A/m (0.1 mT) with the sensitivity range set to 1.0 Hz. The sampling interval was 8 cm with a period of 10 s. The long sampling period ensured acceptable readings for the usually low MS of carbonate sediments. The MS-2 meter measures relative susceptibilities, which need to be corrected for volume variations. For core (d) and coil (D) diameters of 66 and 88 mm, respectively, the corresponding correction factor for d/D is 1.48 (Blum, 1997, p. 38). During data reduction the relative susceptibility is converted to the volume-normalized MS by multiplying by $1/(1.48 \times 10^5)$ or by 0.68×10^{-5} (SI units). Some difficulties occurred when measuring MS on sediments with low susceptibility. In these sediments a trend was seen in which the sediments would appear to have elevated values at the beginning and end of individual sections. Although the problem was not solved, it seems to be related to standardization and data manipulation in the MST software.

NGR is a product of the decay of radioactive atoms, predominantly U, Th, and K. NGR was measured using four scintillation detectors arranged 90° to each other and perpendicular to the core (as outlined by Hoppie et al., 1994). On Leg 182 NGR was measured every 16 cm for a 26-s period. NGR calibration was performed at the beginning of the leg and standards were measured at the end of every site. For the interval at the top of the hole in which pipe remained during downhole logging, the data were used to complete and correct for the attenuation of the gamma-ray wireline log collected through pipe. In open-hole logging sections, the core data were used to calibrate the wireline log.

GRA was used to estimate sediment bulk density. This measurement is based on the principle that the attenuation, mainly by Compton scattering, of a collimated beam of gamma rays (produced by a ^{137}Ce source) passing through a known volume of sediment is related to material density (Boyce, 1976). During Leg 182 the measurement interval was set at 4 cm (4-s period). For each site, GRA and discrete sample bulk densities were compared for repeatability.

Thermal Conductivity

Thermal conductivity during Leg 182 was measured using the needle-probe technique with the TK04 system as described by Blum (1997). For whole cores the probe was inserted through an aperture drilled in the core liner mid-depth in the section. After insertion, the probe was

heated at 3 or 4 W/m and the temperature rise monitored. The optimal integration time for each conductivity measurement is calculated by an algorithm in the TK04 system for time units of 40–300 s and an evaluation time of 240 s. Thermal conductivity was reported in units of watts per meter degrees centigrade (W/m°C) with an accuracy of 5% and a precision of 2%. Data were collected once per core (usually Section 3), increasing to three per core (Sections 1, 3, and 5) when in situ Adara and Davis-Villinger temperature probe (DVTP) measurements were made. For split cores at Site 1129, thermal conductivity measurements samples were first smoothed with emery paper; then the half-space needle cell was tightly secured to the flat surface of the core with Velcro. The sample was then placed in a water bath. Determinations were made using the TK04 system in half-space mode. Heating power was either 2 or 3 W/m for a period of 80 s. Three replicate determinations were made for each sample.

Index Properties

Moisture and density (MAD) measurements (water content, wet and dry bulk density, and grain density) were routinely measured using ~10-cm³ samples from split cores. Porosity and void ratio were calculated from phase-relation equations. Samples for MAD measurements were collected at a frequency of one per section, taking care to sample undisturbed parts of the core and avoid drilling slurry. Sampling frequency was increased as needed to characterize all significant lithologies.

Immediately after samples were collected, wet sediment mass (M_t) was measured. Samples were then placed in a convection oven for 24 hr at a temperature of $105^\circ \pm 5^\circ\text{C}$. After drying, dry sediment mass (M_d) and dry sediment volume (V_d) were measured. Sample mass was determined on board ship to a precision of ± 0.01 g using two Scientech 202 electronic balances to compensate for the ship's motion. Volumes were determined using a helium Quantachrome Penta-Pycnometer with an approximate precision of ± 0.02 cm³. The determination of water content followed the methods of the American Society for Testing and Materials (ASTM) designation (D) 2216 (ASTM, 1989). The recommended equation for the water content calculation, which is the ratio of the pore fluid mass to the dry sediment mass (% dry wt), is as follows:

$$W_c (\% \text{ dry wt}) = (M_t - M_d) / (M_d - rM_t),$$

where W_c is water content reported as a decimal ratio of % dry weight and r is salinity.

Wet bulk density (ρ) is the density of the total sample including pore fluid. In high-porosity sediment, bulk density was calculated using the following:

$$\rho = M_t / V_t,$$

where V_t is the total sample volume (10 cm³).

Porosity (\emptyset) was calculated using the equation

$$\emptyset = (W_c \rho) / [(1 + W_c) \rho_w],$$

where ρ_w is the density of the pore fluid (assuming a salinity of 35‰).

The grain density (ρ_{grain}) was calculated from dry mass and dry volume. Both values were corrected for salt using the equation

$$\rho_{grain} = (M_d - s) / [V_d - (s/\rho_{salt})],$$

where s is salt correction and ρ_{salt} is the density of salt (2.257 g/cm³, assuming a salinity of 35‰).

Dry density (ρ_d) is the ratio of M_d to V_b and is used for calculations of mass accumulation. Dry density was calculated using the equation

$$\rho_d = (\sigma / W_c) \cdot \rho_w.$$

During Leg 182 GRA densimetry measurements on unconsolidated sediments were commonly higher than discrete density measurements. In addition, GRA density in low-porosity sediments was usually lower, as much as 5%, than discrete density measurements. Three explanations for these differences have been proposed (Shipboard Scientific Party, 1997): (1) the MST software does not include a correction for the attenuation effect in high-porosity sediments (Boyce, 1976; Lloyd and Moran, 1992); (2) air trapped in the sediment-filled beakers (unconsolidated sediments) reduces the relative saturated weight and increases the relative volume measured in the pycnometer, thereby decreasing the resulting bulk density; and (3) low-porosity sediments which are semilithified to lithified have a smaller core diameter, and subsequently a relatively smaller attenuating volume than the calibrated volume, which results in a lower calculated density. To solve the first problem, GRA densities were corrected using the Boyce (1976) equation:

$$p = [(p_{bc} - p_{fc})(p_g - p_f)] / (p_{gc} - p_{fc}) + p_f,$$

where p is corrected density, p_{bc} is GRA density, p_{fc} is fluid density calculated from gamma counts (1.128 g/cm³), p_g is the true grain density of quartz (2.65 g/cm³), p_f is the true fluid density (1.024 g/cm³), and p_{gc} is grain density calculated from gamma counts (2.65 g/cm³). It is unclear how to improve the accuracy of the index properties procedure. Therefore, it is assumed that discrete measurements are more accurate, whereas GRA density gives a reliable high-resolution relative density trend.

Beginning with Site 1129, problems were encountered with the pycnometer used for volume measurements. The instrument showed a drift in the volume calibration of individual cells that limited the precision achievable, and duplicate analyses for actual samples showed differences of as much as 10% (e.g., for beaker 547, three determinations gave volumes of 11.39, 12.27, and 11.65 cm³). Calculated grain densities were also very much lower than would be expected for carbonate sediments (average 2.0 ± 0.15 g/cm³; expected density $\cong 2.8$). The cause of this problem is not known, although it may have arisen from an error in calibration of the pycnometer reference cell, or some other malfunction. Index properties measurements at Sites 1129, 1130, 1131, and 1132 (Hole 1132D only) were also affected (see "Physical Properties" in relevant site chapters).

Sonic Velocity

The choice of method and sampling frequency of discrete compressional wave velocity measurements (V_p) was dependent on the degree of consolidation of the sediments.

1. Unconsolidated sediments: V_p was measured using two pairs of perpendicularly oriented digital sound velocimeters (PWS). One pair is aligned vertical to bedding (PWS1; z-direction) and the other is aligned horizontally (PWS2; y-direction) to determine sediment anisotropy. The transducer pairs have a fixed spacing of 7 cm (vertical) and 3.5 cm (horizontal) and were inserted into the split cores of soft sediment. An acoustic signal of 500 kHz was emitted and received by the two transducers. This signal was then digitized by an oscilloscope so that the first-arrival waveform could be manually picked and velocity calculated. Anisotropy could then be determined by the difference between the horizontal and vertical velocity using the following:

$$\text{anisotropy} = 2 \cdot (V_{pt} - V_{pl}) / (V_{pt} + V_{pl}),$$

where V_{pt} is the transverse compressional wave velocity and V_{pl} , the longitudinal velocity. The velocity meter was calibrated by measuring V_p in distilled water. In unconsolidated sediments, at least two P -wave velocity measurements per section were made using either or both PWS1 and PWS2.

V_p in unconsolidated sediments was also measured through the split core (PWS3; x-direction) using vertically oriented transducer pairs (500 kHz), with the upper transducer pressed against the split surface and the lower pressed against the core liner. These data were recorded, digitized, and transferred to a computer as for PWS1 and -2. Core thickness was measured using a digital caliper that was directly mounted on the transducer pair. Zero traveltimes for the velocity transducers were measured using a series of polycarbonate standards of known length. The axial pressure applied between sample and transducer was monitored by a pressure cell. To improve the coupling between transducer and sample, distilled water was applied to the transducer head. Measurements were corrected for the additional traveltime passing through the core liner. In unconsolidated sediments two PWS3 measurements were made per section.

2. Semilithified and consolidated sediments: If sediments were too hard for the PWS1 and -2 transducers to be inserted, only PWS3 data were collected at a frequency of four or more per section.

During the measurements for Site 1127, the pressure cell of PWS3 ceased to operate. No replacement pressure cell was available; thus, an alternate apparatus was constructed that consisted of a pneumatic platform that raised the lower PWS3 transducer a predetermined distance to press the sediment surface against the upper PWS3 transducer. Because there was no way to ensure that the pressure was constant between the transducers and the split core for different samples, pressure differences were minimized by lowering the upper transducer until it made initial contact with the core surface, at which time the lower cell was raised. Despite careful attention to consistency of measurement, there are likely to be slight pressure differences between samples that would result in greater than normal errors in P -wave velocity. Thus, the data from Site

1126 may not be directly comparable to those of subsequent Leg 182 sites. As the new apparatus was being constructed only limited PWS3 measurements could be made at Site 1127, which resulted in a minimal PWS3 data set at this site.

Undrained Shear Strength

The peak undrained and residual shear strength of unconsolidated sediment was measured at an interval of one per section using a Wykeham Farrance motorized vane shear apparatus following the procedures of Boyce (1977). The vane rotation rate was set to 90° per min, and the vane used for all measurements had a 1:1 blade ratio with a dimension of 1.28 cm. This instrument measures the torque and strain at the vane shaft using a torque transducer and potentiometer, respectively. Output for torque and strain were recorded on a Hewlett-Packard X-Y recorder in volts. The shear strength reported was the peak strength determined from the torque vs. strain plot.

In the interpretation of shear vane measurements, a cylinder of sediment is assumed to be uniformly sheared around the axis of the vane in an undrained condition, with cohesion as the principal contributor to shear strength. Departures from this assumption include progressive cracking within and outside of the failing specimen, uplift of the failing core cylinder, drainage of local pore pressures, and stick-slip behavior.

In Situ Temperature Measurements

In situ temperature measurements were made either using an Adara or DVTP temperature tool. The Adara tool fits directly into the coring shoe of the APC and consists of a battery pack, data logger, and a platinum resistance-temperature device calibrated over a temperature range from 0° to 30°C. Before entering the borehole, the tool was first briefly stopped at the mudline to thermally equilibrate with bottom water. After the APC penetrated the sediment, it was held in place for 10 min as the Adara instrument recorded the temperature of the cutting shoe every 5 s. Initially, there was an instantaneous temperature rise from frictional heating caused by APC penetration. This heat gradually dissipated into the surrounding sediments, and the equilibrium temperature of the sediments was then estimated by applying a mathematical heat-conduction model to the temperature decay record (Horai and Von Herzen, 1985). Additional information on the Adara tool can be found in previous *Initial Reports* volumes (Shipboard Scientific Party, 1992, 1994).

The DVTP tool is used in semilithified sediments in which the APC cannot penetrate and, unlike the Adara, the DVTP requires a separate wireline run. This tool measures formation temperature using a probe that is pushed into the top of the sediment section. The probe is conical with two thermistors, one located 1 cm from the tip of the probe and the other 12 cm above the tip. A third thermistor, referred to as the internal thermistor, is located in the electronics package. Thermistor sensitivity is 1 mK in an operating range from -5° to 20°C, and the total operating range is -5° to 100°C. The thermistors were calibrated at the factory and on the laboratory bench before installation in the probe. In addition to the thermistors, the probe contains an accelerometer sensitive to 0.98 m/s². Both peak and mean acceleration are recorded by the logger. The accelerometer data are used to track disturbances to the instrument package during the equilibration interval.

In a DVTP deployment, mudline temperatures are measured for 10 min on the first run within each hole and 2 min for subsequent runs before descent into the hole for a 10-min equilibration interval in the bottom. Mudline temperatures are also collected for at least 2 min on ascent. Data from the probe tip thermistor were used for estimation of in situ temperatures.

For shallow-water sites a longer mudline stop was required to ensure that the temperature tools had sufficient time to equilibrate to bottom-water temperatures. At deeper sites this time was reduced as the tools are able to thermally equilibrate during descent through deeper waters with very low thermal gradients. This problem is less serious with the DVTP because it has a lower heat capacity and a thermal time constant that is less than the Adara temperature shoe.

Data reduction procedures are similar for both temperature tools. The synthetic thermal decay curves for the Adara tool and DVTP are a function of the geometry and thermal properties of the probe and the sediments (Bullard, 1954; Horai and von Herzen, 1985). However, it is never possible to obtain a perfect match between the synthetic curves and the data because (1) the probe never reaches thermal equilibrium during the penetration period; (2) contrary to theory, the frictional pulse upon insertion is never instantaneous; and (3) temperature data are sampled at discrete intervals, meaning that the exact time of penetration is always uncertain. Thus, both the effective penetration time and equilibrium temperature must be estimated by applying a fitting procedure, which involves shifting the synthetic curves in time to obtain a match with the recorded data. The data collected >20–50 s after penetration usually provide a reliable estimate of equilibrium temperature. However, where the APC has not achieved a full stroke, leakage of drilling fluid into the formation may occur and results are not considered reliable.

DOWNHOLE MEASUREMENTS

Logging Procedures and Logging Data

Introduction

Downhole logging on board the *JOIDES Resolution* is provided by Lamont-Doherty Earth Observatory Borehole Research Group (LDEO-BRG) in conjunction with Leicester University Borehole Research (LUBR), the Laboratoire de Mesures en Forage (LMF), and Schlumberger Well Logging Services. During Leg 182, the high-resolution temperature/acceleration/pressure tool (LDEO-TAP) replaced the Lamont temperature tool (LDEO-TLT) as the borehole temperature tool.

Borehole Preparation

Before logging, most holes were first flushed of debris by circulating heavy viscous drilling fluid (sepiolite mud and seawater) through the hole. The bottom-hole assembly (BHA) was then pulled up to 80–110 mbsf and run down the hole again to ream out borehole irregularities and stabilize borehole walls. The hole was then filled with a sepiolite mud pill, and the BHA was raised to 80–110 mbsf.

Data Recording and Processing

Data for each logging run were recorded and stored digitally and monitored in real time using the Schlumberger Multitask Acquisition and Imaging System (MAXIS 500). Upon the completion of logging at each hole, data were transferred to the shipboard Downhole Measurements Laboratory for preliminary processing and interpretation. Formation MicroScanner (FMS) image data were interpreted using Schlumberger's GeoFrame 3.1.2 software package.

Logging data were transmitted for processing to LDEO-BRG using a satellite high-speed data link after each hole was logged. Data processing at LDEO-BRG included (1) depth-shifting of all logs relative to a common datum (i.e., mbsf), (2) corrections specific to individual tools, and (3) quality control and rejection of unrealistic or spurious values. Once processed at LDEO-BRG, log data were transmitted back to the ship. Log curves of LDEO-BRG processed data were then replotted on board and used to refine interpretations. Further postcruise processing of the log data from the FMS and the geologic high-resolution magnetic tool (GHMT) is performed at LDEO-BRG, at LMF in Aix-en-Provence, France.

Postcruise-processed acoustic, caliper, density, gamma-ray, magnetic, neutron porosity, resistivity, and temperature data in ASCII format are available (see the "[Related Leg Data](#)" contents list).

Log Data Quality

A major factor influencing the quality of log data is the condition of the borehole. If the borehole diameter is variable over short intervals, resulting from washouts during drilling, clay swelling, or borehole wall collapse, there may be data acquisition problems for tools that require good contact with the wall (i.e., FMS, density, and porosity logging tools). Measurements that do not require contact with the borehole wall, such as resistivity and sonic velocity, are generally less sensitive to borehole conditions. The quality of boreholes was improved by minimizing the circulation of drilling fluid, flushing the borehole to remove debris, and logging as soon as possible after drilling and conditioning were completed. Factors affecting data quality for each tool are discussed in the following section.

Log Depth Scales

The depth of each logged measurement is calculated from the length of the logging cable, minus the cable length to the seafloor (seafloor is identified by an abrupt reduction in gamma-ray counts at the water/sediment interface). Discrepancies between the core depth and the log depth may occur because of core expansion, incomplete core recovery, and drill-pipe stretch in the case of core depth, and incomplete heave compensation, cable stretch (1 m/km), and cable slip in the case of log depth. Tidal changes in sea level may also have an effect. Thus, there may be significant differences between drill-pipe depth and cable depth that should be considered when using the logs.

Logging Tools and Tool Strings

Logging Tool Strings

During Leg 182 individual logging tools were combined into the following four different logging strings (Fig. F10; Table T8):

1. The triple combination (porosity, density, and resistivity) tool string, composed of the phasor dual induction-spherically focused resistivity tool (DITE-SFL), the hostile environment litho-density sonde (HLDS), the accelerator porosity sonde (APS), and the hostile environment natural gamma-ray sonde (HNGS). The LDEO-TAP was attached to the base of this tool string.
2. The FMS/sonic tool string, composed of the FMS, the general-purpose inclinometer tool (GPIT), and the sonic digital tool (SDT). The natural gamma-ray tool (NGT) was included at the top of this tool string.
3. The GHMT, composed of the high-sensitivity total magnetic field sensor (nuclear magnetic resonance sonde [NMRS]) and the susceptibility magnetic sonde (SUMS). The NGT was again positioned at the top of this tool string. During Leg 182 the NMRS was not operating and total magnetic field was not measured.
4. The well seismic tool (WST).

Data from the NGT or HNGS placed at the top of all but the WST tool string provides a common basis for correlating between logging runs and depth shifting of logs.

Logging Tools

Brief descriptions of individual logging tools used during Leg 182, including their geological applications and the controls on data quality, are given below. Properties of the formation measured by each tool, sample intervals used, and precision of the measurements made (including the vertical resolution and depth of investigation at typical logging speeds) are summarized in Table T8. Explanations of tool name acronyms, the acronyms by which the log data generated by the different tools are referred, and their units of measurement are summarized in Table T9.

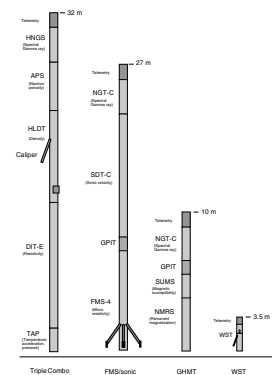
More detailed descriptions of individual logging tools and their geological applications can be found in Ellis (1987), Goldberg (1997), Lovell et al. (1998), Rider (1996), Schlumberger (1989, 1994a, 1994b, 1995), Serra (1984, 1986, 1989), Timur and Toksöz (1985) and the LDEO-BRG Wireline Logging Services Guide (1994).

Natural Gamma-Ray Tool (NGT)

The NGT uses a sodium iodine (NaI) scintillation detector to measure total formation NGR emissions (K + U + Th in American Petroleum Institute [API] units) and utilizes five-window spectroscopy to determine concentrations of radioactive K, Th, and U. The NGT also provides a measure of the uranium-free or computed gamma ray (K + Th in API units).

The NGT response is influenced by borehole diameter and the weight and concentration of bentonite or KCl present in the drilling mud. KCl may be added to the drilling mud to prevent fresh-water clays from

F10. Configurations of tool strings, p. 55.



T8. Logging tools, p. 70.

T9. Logging tool and measurement acronyms, and units of measurement, p. 71.

swelling and forming obstructions. All these effects are corrected for during processing of NGT data at LDEO-BRG.

Hostile Environment Natural Gamma-Ray Sonde (HNGS)

The HNGS uses a measurement principle similar to that of the NGT described above. However, the HNGS uses two bismuth germanate scintillation detectors for gamma-ray detection with full spectral processing, significantly improving tool precision compared to the NGT. The spectral analysis filters out gamma-ray energies below 500 keV, eliminating sensitivity to bentonite or KCl in the drilling mud, and improves measurement accuracy. The HNGS generates the same output as the NGT, as well as estimating the average borehole potassium contribution to the total potassium signal. Log data from the HNGS are corrected for variability in borehole size and borehole potassium concentrations on board ship.

Hostile Environment Lithodensity Sonde (HLDS)

The HLDS consists of a radioactive cesium (^{137}Cs) gamma-ray source (622 keV) and far and near gamma-ray detectors mounted on a shielded skid that is pressed against the borehole wall by a hydraulically activated eccentricizing arm. Gamma radiation emitted by the source undergoes both Compton scattering and photoelectric absorption. Compton scattering involves the transfer of energy from gamma rays to the electrons in the formation via elastic collision. The number of scattered gamma rays that reach the detectors is directly related to the number of electrons in the formation, which is in turn related to bulk density. Porosity may also be derived from this bulk density if the matrix density is known.

The HLDS also measures the photoelectric effect (PEF) caused by absorption of low-energy gamma rays. Photoelectric absorption occurs when gamma rays have energies <150 keV after being repeatedly scattered by the electrons in the formation. Because PEF depends on the atomic number of elements in the formation, it is essentially independent of porosity. Thus, PEF varies according to the chemical composition of the sediment. For example, the PEF of pure calcite = 5.08 barn/e⁻; illite = 3.03 barn/e⁻; quartz = 1.81 barn/e⁻; and kaolinite = 1.49 barn/e⁻. The PEF values can be used in combination with NGT curves to identify different types of clay minerals. Failure to maintain good contact between the tool and borehole wall is essential for good HLDS logs as poor contact will result in an underestimation of density values.

Accelerator Porosity Sonde (APS)

The APS consists of a minitron neutron generator that produces fast neutrons (14.4 MeV), and five neutron detectors (four epithermal and one thermal), positioned at different spacings along the tool. The tool is pressed against the borehole wall by an eccentricizing bow-spring. Emitted fast neutrons are slowed by collisions, especially with hydrogen nuclei (because of the large thermal neutron-capture cross sections of hydrogen nuclei), which are mainly present in the pore water. Upon degrading to thermal energies (0.025 eV), the neutrons are captured by the nuclei of Si, Cl, B, (silica, chloride, and boron), and other elements, resulting in a gamma-ray emission. The neutron detectors record both the numbers of neutrons arriving at various distances from the source

and neutron arrival times, which act as a measure of formation porosity. If the concentration of water is low, as in low-porosity formations, neutrons travel further before being captured. This results in a high count rate. Data from the APS are used to derive (1) near and far epithermal neutron porosity (0.1–100 eV); (2) thermal (<0.025 eV) neutron measurement of the formation-capture cross section (σ_f), which is a useful indicator of B, Cl, and rare-earth elements that may be present in shales and possibly dolomite; and (3) corrections for borehole irregularities and tool stand-off. The presence of clay minerals containing hydrogen may result in an overestimation of porosity with this tool. In addition, incomplete contact with the borehole wall causes the tool to detect borehole water, giving an overestimation of porosity. The HNGS, APS, and the HLDS are collectively called the integrated porosity-lithology tool.

Phasor Dual Induction–Spherically Focused Resistivity Tool (DITE-SFL)

The DITE-SFL provides measurements of three different resistivity values: (1) deep induction, (2) medium induction, and (3) shallow spherically focused resistivity (SFLU). Resistivity is controlled mainly by the conductivity of pore fluids and by the amount and connectivity of pores. Two induction devices transmit high-frequency alternating currents through transmitter coils, creating a magnetic field that induces secondary (Foucault) currents in the formation. These currents produce a new inductive signal proportional to formation conductivities that are recorded by the receiving coils. The measured conductivities are then converted to resistivity (Ωm). The SFLU measures the current necessary to maintain a constant voltage drop across a fixed interval and gives a direct measurement of resistivity.

LDEO High-Resolution Temperature/Acceleration/Pressure Tool (LDEO-TAP)

The LDEO-TAP is a “dual application” logging tool (i.e., it can operate as either a wireline tool or as a memory tool using the same sensors and data acquisition electronics, depending on the purpose and required precision of logging data). The full specifications of this new tool are described in Table T10. During Leg 182 the LDEO-TAP was deployed as a memory tool in low-resolution mode, with the data being stored in the tool and then downloaded after the logging run was completed. The LDEO-TAP offers greater flexibility in logging operations, and it substantially improves the quality and resolution of data over an extended ambient temperature range (when used in the wireline mode) compared to the superseded LDEO-TLT.

The tool automatically starts recording after a preset pressure (depth) has been reached. Temperature, measured by high-precision thermistors, and pressure are measured every second. Tool acceleration is recorded four times per second. Data are recorded as a function of time and correlated to depth on the basis of a synchronized time-wireline cable depth record and pressure recordings. After logging, data are downloaded via a modem. Temperatures determined using the LDEO-TAP do not represent in situ formation temperatures because water circulation during drilling will have disturbed temperature conditions in the borehole. However, abrupt temperature changes superimposed on the overall measured gradient may represent localized fluid flow into the

T10. LDEO-TAP tool specifications, p. 72.

borehole (indicative of fluid pathways and fracturing) and/or changes in permeability at lithologic boundaries.

Sonic Digital Tool (SDT)

The SDT measures the time required for sound to travel through the formation between a transmitter and a receiver. As this tool averages replicate analyses, it provides direct measurements of sound velocity through the sediments that are relatively free from the effects of formation damage and borehole enlargement (Schlumberger, 1989).

The SDT contains two broadband piezoelectric ceramic transmitters and receivers spaced 61 cm apart, with the lower receiver located 91 cm above the upper transmitter. In addition, eight wideband ceramic receivers are arranged in an array 1.07 m long and 2.44 m above the upper transmitter at the base of the sonde. This configuration provides a total of eight different transit-time measurements. Interval transit times are converted to compressional wave velocities (km/s). Full waveforms are recorded by the tool, allowing shorebased postprocessing to estimate shear- and Stoneley-wave velocities, as well as amplitude attenuation. Logs are edited for cycle skipping and obviously spurious values.

Formation MicroScanner (FMS)

The FMS produces high-resolution images of borehole wall microresistivity. This tool has four orthogonally oriented pads, each having 16 button electrodes that are pressed against the borehole walls. Good contact with the borehole wall is necessary for high-quality data. During a single pass, ~30% of the borehole wall is imaged. Coverage may be increased by a second run. However, there is no active way of orienting the pads in the borehole; therefore, there is no control over differences in coverage between the first and second pass. The current-intensity measurements in each button are converted to variable-intensity color images that reflect microresistivity variations. The vertical resolution of FMS images is claimed by Schlumberger to be ~5 mm, but is probably lower (~1 cm) in practice.

FMS images are oriented to magnetic north using the GPIT. This allows the dip and strike of geological features intersecting the hole to be measured from processed FMS images. FMS images can be used to visually compare logs with core and ascertain the orientations of bedding, fracture patterns, and sedimentary structures. Comparatively small-scale features, such as burrows and vugs, can also be identified using FMS images.

FMS images have proved particularly valuable in the interpretation of sedimentary structures in previous ODP legs and have been used to identify cyclical stacking patterns in carbonates (Eberli, Swart, Malone, et al., 1997), soft sediment slumping (Norris, Kroon, Klaus, et al., 1998), turbidite deposits (Lovell et al., 1998), cross-beds (Hiscott et al., 1992), and facies changes (Serra, 1989). Detailed processing of FMS images in combination with other log and core data is performed postcruise at LDEO-BRG, LUBR, and LMF.

General-Purpose Inclinometer Tool (GPIT)

The GPIT was included in the FMS/sonic tool string to calculate tool acceleration and orientation during logging. The GPIT contains a triple-axis accelerometer and a triple-axis magnetometer. The GPIT records

the orientation of the FMS images and allows more precise determination of log depths than can be determined from cable length, which may experience stretching and/or be affected by ship heave.

Geologic High-Resolution Magnetic Tool (GHMT)

The GHMT normally consists of a high-sensitivity total magnetic field sensor (NMRS) coupled with a MS sensor (SUMS). However, during Leg 182 the NMRS was not functioning. The SUMS measures MS by means of low-frequency induction in the surrounding sediment.

Well Seismic Tool (WST)

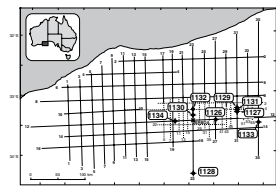
The WST was used to produce zero-offset check shots in the borehole. The WST consists of a single geophone used to record the full waveform of acoustic waves generated by a seismic source positioned just below the sea surface. During Leg 182 a 45/105-in³ generator-injector (GI) gun was used as the seismic source positioned at a water depth of 3 m and offset from the borehole by 50 m on the port side of the *JOIDES Resolution*. The WST was held against the borehole wall at variable intervals, and the GI gun was typically fired between 8 and 15 times at each station. The recorded waveforms were stacked and a one-way traveltime determined from the median of the first breaks measured; thus providing check shots for calibration of the integrated transit time calculated from sonic logs (see “[Seismic Stratigraphy](#),” p. 31). Check shot calibration is required for the borehole to seismic tie because *P*-wave velocities derived from the sonic log may differ significantly from seismic stacking velocities and velocities obtained via well seismic surveys. These differences result from (1) differential frequency dispersion (the sonic tool operates at 10–20 kHz, seismic data in the 50–100 Hz range), (2) difference in travel paths between well seismic and surface seismic surveys, and (3) borehole effects caused by formation alterations (Schlumberger, 1989). In addition, sonic logs cannot be measured through pipe and the traveltime to the uppermost logging point must be estimated by other means.

SEISMIC STRATIGRAPHY

Multichannel Seismic Database

Present knowledge of the western Great Australian Bight seismic stratigraphy is based on extensive, high-quality multichannel seismic reflection data, together with a single oil exploration drill hole (Jerboa-1), which provides minimal information about the Cenozoic succession (Fig. F11). Characteristics of the various seismic data sets are summarized in Table T11. The original Leg 182 drilling proposals (James and Feary, 1993; Feary et al., 1994, 1995) were based on detailed seismic stratigraphic interpretation (Feary and James, 1998, reprinted as [Chap. 2](#)) of a grid of 2350 km of high-quality, regional two-dimensional seismic reflection lines collected and processed by the Japan National Oil Corporation (JNOC) in 1990 and 1991, over an area of 155,000 km² on the continental shelf and upper slope of the western Great Australian Bight. An additional 1380 km of moderate-quality regional two-dimensional seismic lines collected by Esso Australia in 1979 and reprocessed by JNOC were also used to fill gaps in the JNOC data set.

F11. Map of the western Great Australian Bight showing Leg 182 drill sites, [p. 56](#).



T11. Acquisition parameters used to establish regional seismic stratigraphy in the western Great Australian Bight, [p. 73](#).

In February 1996 the Australian Geological Survey Organisation (AGSO) performed a multichannel seismic site-survey cruise (Feary, 1995) on the *Rig Seismic* in support of the Leg 182 drilling proposal (Fig. F12). This cruise collected 1800 line-kilometers of high-resolution, two-dimensional seismic data as 0.5-nmi-spaced grids centered on each site, together with tie lines between sites (individual site-survey seismic grid maps are presented in the “Seismic Stratigraphy” sections of the site chapters). The Australian Geological Survey Organisation Survey 169 (AGSO169) data were collected using a 1000-m 80-channel analog streamer, using Seismic Systems Inc. GI air guns deployed in full bubble-suppression mode (configured with 45-in³ generator and 105-in³ injector chambers). A single array of three GI guns was used in shallow water (<750 m) and twin arrays of three GI guns were used in deep water (750–4500 m), running at 2000 psi (effectively 1800 ± 200 psi) at 3 m depth. Data are 3.5-s records in shallow water and 8.5-s records in deep water (12.5-m shot interval in shallow water, 25-m shot interval in deep water), with a 1-ms sample rate. Data acquisition specifications were in accordance with current exploration industry standards. Primary and independent backup differential Global Positioning System navigation systems resulted in extremely high navigational accuracy, and excellent weather conditions resulted in low streamer noise levels (normally 5–10 µB).

Seismic Interpretation

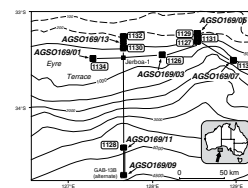
The regional Cenozoic seismic stratigraphy (Feary and James, 1998, reprinted as Chap. 2), derived from interpretation of the JNOC regional seismic data set, is based on division of the Cenozoic succession into seven unconformity-bounded seismic sequences. The high-resolution site-survey data set permitted the identification of additional unconformity surfaces within many of the regional seismic sequences; however, as there is insufficient resolution to extend these boundaries regionally, they are traced on an individual site basis only.

Interpretation of the stacked and migrated two-dimensional seismic data was performed on a GeoQuest IESX-2D seismic interpretation workstation during the precruise proposal and safety evaluation processes. A GeoQuest workstation with the complete seismic and interpretation data sets was available on board throughout the leg, so it was possible to evaluate coring results during drilling to aid in operational decisions and to contribute to data interpretations. In particular, it was possible to immediately derive the detailed characteristics of seismic sequences intersected at each site (presented in the “Seismic Stratigraphy” sections of the site chapters) and to make limited predictions based on the results of earlier sites. The availability of the workstation with the complete interpretation package was invaluable when drilling difficulties prevented successful coring in Holes 1129A and 1129B at the original Site 1129 location, and provided the basis for siting the successful Holes 1129C and 1129D 0.5 nmi south of the original location.

Correlation of Borehole Data and Seismic Reflection Profiles

Correlation of two-dimensional seismic reflection profiles to one-dimensional data derived from cores or downhole logs is a key step toward understanding drilling results within a regional context (Mayer,

F12. Map showing Leg 182 drill sites relative to AGSO169, p. 57.



1994). The principal requirement for such correlation is to establish the relationship between the two-way-traveltime scale of seismic reflection data displays and the depth scale of coring. Check-shot surveys provide the optimum time–depth control to calibrate integrated sonic curves derived from interval transit-time data and to provide individual time–depth tie points. Before Leg 182, stacking velocity functions derived during seismic reflection data processing were used to estimate depths to drilling targets. The procedure undertaken during Leg 182 was for processed check-shot results (WST; see “[Downhole Measurements](#),” p. 25) to be plotted on depth to two-way-traveltime graphs to determine the relationship between depths of lithofacies and/or biostratigraphic boundaries encountered during coring, and sequence boundaries and horizons located on seismic data. Because sonic logs only provide data up to the base of drill pipe, the integrated sonic trace derived from interval transit-time data was unconstrained within the time domain. Check-shot tie points provided the necessary time constraint so that the integrated sonic trace could define the actual time–depth relationship at each site. Check-shot results were also used to compare the final time–depth relationship with predictions based on stacking velocities. These plots show that the actual time–depth relationship defined by check-shot surveys occurred close to or at the lower limit of the envelopes defined by stacking velocity curves, indicating that stacking velocities consistently underestimate actual sediment velocities. Where check-shot surveys were not run, this consistent relationship between stacking and sediment velocities was used to produce an optimum time–depth estimate, with the integrated sonic trace being placed close to the lower limit of the envelopes defined by stacking velocity curves.

REFERENCES

- ASTM, 1989. Standard test method for laboratory miniature vane shear test for saturated fine-grained clayey soil. *Annual Book of ASTM Standards* (Vol. 04.08): Philadelphia (Am. Soc. Testing and Mater.), D4648-87:868–873.
- Backman, J., 1986. Late Paleocene to middle Eocene calcareous nannofossil biochronology from the Shatsky Rise, Walvis Ridge and Italy. *Palaeogeogr., Palaeoclimatol., Palaeoecol.*, 57:43–59.
- , 1987. Quantitative calcareous nannofossil biochronology of middle Eocene through early Oligocene sediment from DSDP Sites 522 and 523. *Abh. Geol. Bundesanst. (Austria)*, 39:21–31.
- Berggren, W.A., 1969. Rates of evolution in some Cenozoic planktonic foraminifera. *Micropaleontology*, 15:351–365.
- , 1993. Neogene planktonic foraminiferal biostratigraphy of eastern Jamaica. *Mem.—Geol. Soc. Am.*, 182:179–217.
- Berggren, W.A., Hilgen, F.J., Langereis, C.G., Kent, D.V., Obradovich, J.D., Raffi, I., Raymo, M.E., and Shackleton, N.J., 1995a. Late Neogene chronology: new perspectives in high-resolution stratigraphy. *Geol. Soc. Am. Bull.*, 107:1272–1287.
- Berggren, W.A., Kent, D.V., Obradovich, J.D., and Swisher, C.C., III, 1992. Towards a revised Paleogene geochronology. In Prothero, D.R., and Berggren, W.A. (Eds.), *Eocene-Oligocene Climatic and Biotic Evolution*: Princeton (Princeton Univ. Press), 29–45.
- Berggren, W.A., Kent, D.V., Swisher, C.C., III, and Aubry, M.-P., 1995b. A revised Cenozoic geochronology and chronostratigraphy. In Berggren, W.A., Kent, D.V., Aubry, M.-P., and Hardenbol, J. (Eds.), *Geochronology, Time Scales and Global Stratigraphic Correlation*. Spec. Publ.—Soc. Econ. Paleontol. Mineral., 54:129–212.
- Berggren, W.A., Kent, D.V., and Flynn, J.J., 1985a. Jurassic to Paleogene, Part 2. Paleogene geochronology and chronostratigraphy. In Snelling, N.J. (Ed.), *The Chronology of the Geological Record*. Geol. Soc. London Mem., 10:141–195.
- Berggren, W.A., Kent, D.V., and Van Couvering, J.A., 1985b. The Neogene, Part 2. Neogene geochronology and chronostratigraphy. In Snelling, N.J. (Ed.), *The Chronology of the Geological Record*. Geol. Soc. London Mem., 10:211–260.
- Berggren, W.A., and Miller, K.G., 1988. Paleogene tropical planktonic foraminiferal biostratigraphy and magnetobiochronology. *Micropaleontology*, 34:362–380.
- Blow, W.H., 1969. Late middle Eocene to Recent planktonic foraminiferal biostratigraphy. In Brönnimann, P., and Renz, H.H. (Eds.), *Proc. First Int. Conf. Planktonic Microfossils, Geneva, 1967*: Leiden (E.J. Brill), 1:199–422.
- , 1979. *The Cainozoic Globigerinida*: Leiden (E.J. Brill).
- Blum, P., 1997. Physical properties handbook: a guide to the shipboard measurements of physical properties of deep-sea cores. *ODP Tech. Note*, 26.
- Bolli, H.M., and Saunders, J.B., 1985. Oligocene to Holocene low latitude planktic foraminifera. In Bolli, H.M., Saunders, J.B., and Perch-Nielsen, K. (Eds.), *Plankton Stratigraphy*: Cambridge (Cambridge Univ. Press), 155–262.
- Bone, Y., and James, N.P., 1993. Bryozoans as carbonate sediment producers on the cool-water Lacepede Shelf, Southern Australia. *Sediment. Geol.*, 86:247–271.
- Boyce, R.E., 1976. Definitions and laboratory techniques of compressional sound velocity parameters and wet-water content, wet-bulk density, and porosity parameters by gravimetric and gamma-ray attenuation techniques. In Schlanger, S.O., Jackson, E.D., et al., *Init. Repts. DSDP*, 33: Washington (U.S. Govt. Printing Office), 931–958.
- , 1977. Deep Sea Drilling Project procedures for shear strength measurement of clayey sediment using modified Wykeham Farrance laboratory vane apparatus. In Barker, P.F., Dalziel, I.W.D., et al., *Init. Repts. DSDP*, 36: Washington (U.S. Govt. Printing Office), 1059–1068.

- Bukry, D., 1973. Low-latitude coccolith biostratigraphic zonation. *In* Edgar, N.T., Saunders, J.B., et al., *Init. Repts. DSDP*, 15: Washington (U.S. Govt. Printing Office), 685–703.
- , 1975. Coccolith and silicoflagellate stratigraphy near Antarctica, Deep Sea Drilling Project, Leg 28. *In* Hayes, D.E., Frakes, L.A., et al., *Init. Repts. DSDP*, 28: Washington (U.S. Govt. Printing Office), 709–723.
- Bullard, E.C., 1954. The flow of heat through the floor of the Atlantic Ocean. *Proc. R. Soc. London A*, 222:408–429.
- Cande, S.C., and Kent, D.V., 1995. Revised calibration of the geomagnetic polarity timescale for the Late Cretaceous and Cenozoic. *J. Geophys. Res.*, 100:6093–6095.
- Chaisson, W.P., and Leckie, R.M., 1993. High-resolution Neogene planktonic foraminifer biostratigraphy of Site 806, Ontong Java Plateau (western equatorial Pacific). *In* Berger, W.H., Kroenke, L.W., Mayer, L.A., et al., *Proc. ODP, Sci. Results*, 130: College Station, TX (Ocean Drilling Program), 137–178.
- Chaproniere, G.C.H., Shafik, S., Truswell, E.M., MacPhail, M.K., and Partridge, A.D., 1995. Cainozoic. *In* *Australian Phanerozoic Time Scale*. Aust. Geol. Surv. Org., 10.
- Chaproniere, G.C.H., Styzen, M.J., Sager, W.W., Nishi, H., Quinterno, P.J., and Abrahamsen, N., 1994. Late Neogene biostratigraphic and magnetostratigraphic synthesis, Leg 135. *In* Hawkins, J., Parson, L., Allan, J., et al., *Proc. ODP, Sci. Results*, 135: College Station, TX (Ocean Drilling Program), 857–877.
- Coccioni, R., Monaco, P., Monechi, S., Nocchi, M., and Parisi, G., 1988. Biostratigraphy of the Eocene-Oligocene boundary at Massignano (Ancona, Italy). *In* Premoli Silva, I., Coccioni, R., and Montanari, A. (Eds.), *The Eocene-Oligocene Boundary in the Marche-Umbria Basin (Italy)*. Int. Subcomm. Paleogr. Strat., Eocene/Oligocene Meeting, Spec. Publ., II, 1:59–80.
- Curry, W.B., Shackleton, N.J., Richter, C., et al., 1995. *Proc. ODP, Init. Repts.*, 154: College Station, TX (Ocean Drilling Program).
- Droser, M.L., and Bottjer, D.J., 1986. A semiquantitative field classification of ichnofabric. *J. Sediment. Petrol.*, 56:558–559.
- Dunham, R.J., 1962. Classification of carbonate rocks according to depositional texture. *In* Ham, W.E. (Ed.), *Classification of Carbonate Rocks*. AAPG Mem., 108–121.
- Eberli, G.P., Swart, P.K., Malone, M.J., et al., 1997. *Proc. ODP, Init. Repts.*, 166: College Station, TX (Ocean Drilling Program).
- Ellis, D.V., 1987. *Well Logging for Earth Scientists*: New York (Elsevier).
- Embry, A.F., and Klovan, J.E., 1971. A late Devonian reef tract on northeastern Banks Island, Northwest Territories. *Bull. Can. Pet. Geol.*, 19:730–781.
- Emeis, K.-C., and Kvenvolden, K.A., 1986. Shipboard organic geochemistry on *JOIDES Resolution*. *ODP Tech. Note*, 7.
- Espitalié, J., Deroo, G., and Marquis, F., 1986. La pyrolyse Rock-Eval et ses applications, Partie III. *Rev. Inst. Fr. Pet.*, 41:73–89.
- Feary, D.A., 1995. Proposal for an ODP site survey cruise by the R/V Rig Seismic in the western Great Australian Bight. *Aust. Geol. Surv. Org.*, 67.
- Feary, D.A., and James, N.P., 1998. Seismic stratigraphy and geological evolution of the Cenozoic, cool-water, Eucla Platform, Great Australian Bight. *AAPG Bull.*, 82:792–816.
- Feary, D.A., James, N.P., and McGowran, B., 1994. Cenozoic cool-water carbonates of the Great Australian Bight: reading the record of Southern Ocean evolution, sea level, paleoclimate, and biogenic production. *Aust. Geol. Surv. Org.*, 62.
- Feary, D.A., James, N.P., McGowran, B., and Smart, P.L., 1995. Cenozoic cool-water carbonates of the Great Australian Bight: reading the record of Southern Ocean evolution, sealevel, paleoclimate, and biogenic production. *Aust. Geol. Surv. Org.*, 78.
- Gartner, S., 1992. Miocene nannofossil chronology in the North Atlantic, DSDP Site 608. *Mar. Micropaleontol.*, 18:307–331.

- Gealy, E.L., Winterer, E.L., and Moberly, R., Jr., 1971. Methods, conventions, and general observations. *In* Winterer, E.L., Riedel, W.R., et al., *Init. Repts. DSDP*, 7 (Pt. 1): Washington (U.S. Govt. Printing Office), 9–26.
- Gersonde, R., Hoddell, D.A., Blum, P., et al., 1999. *Proc. ODP, Init. Repts.*, 177. College Station, TX (Ocean Drilling Program).
- Gieskes, J.M., Gamo, T., and Brumsack, H., 1991. Chemical methods for interstitial water analysis aboard *JOIDES Resolution*. *ODP Tech. Note*, 15.
- Glaçon, G., Vergnaud Grazzini, C., Iaccarino, S., Rehault, J.-P., Randrianasolo, A., Sierro, J.F., Weaver, P., Channell, J., Torii, M., and Hawthorne, T., 1990. Planktonic foraminiferal events and stable isotope records in the upper Miocene, Site 654. *In* Kastens, K.A., Mascle, J., et al., *Proc. ODP, Sci. Results*, 107: College Station, TX (Ocean Drilling Program), 415–427.
- Goldberg, D., 1997. The role of downhole measurements in marine geology and geophysics. *Rev. Geophys.*, 35:315–342.
- Hagelberg, T., Shackleton, N., Pisias, N., and Shipboard Scientific Party, 1992. Development of composite depth sections for Sites 844 through 854. *In* Mayer, L., Pisias, N., Janecek, T., et al., *Proc. ODP, Init. Repts.*, 138 (Pt. 1): College Station, TX (Ocean Drilling Program), 79–85.
- Hagelberg, T.K., Pisias, N.G., Shackleton, N.J., Mix, A.C., and Harris, S., 1995. Refinement of a high-resolution, continuous sedimentary section for studying equatorial Pacific Ocean paleoceanography, Leg 138. *In* Pisias, N.G., Mayer, L.A., Janecek, T.R., Palmer-Julson, A., and van Andel, T.H. (Eds.), *Proc. ODP, Sci Results*, 138: College Station, TX (Ocean Drilling Program), 31–46.
- Hiscott, R.N., Colella, A., Pezard, P., Lovell, M.A., and Malinverno, A., 1992. Sedimentology of deep-water volcanoclastics, Oligocene Izu-Bonin forearc basin, based on formation microscanner images. *In* Taylor, B., Fujioka, K., et al., *Proc. ODP, Sci. Results*, 126: College Station, TX (Ocean Drilling Program), 75–96.
- Hooton, D.H., and Giorgetta, N.E., 1977. Quantitative x-ray diffraction analysis by a direct calculation method. *X-Ray Spectrom.*, 6:2–5.
- Hoppie, B.W., Blum, P., and the Shipboard Scientific Party, 1994. Natural gamma-ray measurements on ODP cores: introduction to procedures with examples from Leg 150. *In* Mountain, G.S., Miller, K.G., Blum, P., et al., *Proc. ODP, Init. Repts.*, 150: College Station, TX (Ocean Drilling Program), 51–59.
- Horai, K., and Von Herzen, R.P., 1985. Measurement of heat flow on Leg 86 of the Deep Sea Drilling Project. *In* Heath, G.R., Burckle, L.H., et al., *Init. Repts. DSDP*, 86: Washington (U.S. Govt. Printing Office), 759–777.
- Hornibrook, N. de B., Brazier, R.C., and Strong, C.P., 1989. Manual of New Zealand Permian to Pleistocene foraminiferal biostratigraphy. *N. Z. Geol. Surv. Paleontol. Bull.*, 56:1–175.
- James, N.P., and Feary, D.A., 1993. Great Australian Bight: evolution of a Cenozoic carbonate continental margin. *Ocean Drilling Program, Proposal 367-Rev.*
- Jansen, E., Raymo, M.E., Blum, P., et al., 1996. *Proc. ODP, Init. Repts.*, 162: College Station, TX (Ocean Drilling Program).
- Jenkins, D.G., 1971. New Zealand Cenozoic planktonic foraminifera. *N. Z. Geol. Surv. Paleontol. Bull.*, 42:1–277.
- , 1985. Southern mid-latitude Paleocene to Holocene planktic foraminifera. *In* Bolli, H.M., Saunders, J.B., and Perch-Nielsen, K. (Eds.), *Plankton Stratigraphy*: Cambridge (Cambridge Univ. Press), 263–282.
- , 1993. Cenozoic Southern mid- and high-latitude biostratigraphy and chronostratigraphy based on planktonic foraminifera. *In* Kennett, J.P., and Warnke, D.A. (Eds.), *The Antarctic Paleoenvironment: A Perspective on Global Change*. *Antarct. Res. Ser.*, 60:125–144.
- Joyce, J.E., Tjalsma, L.R.C., Prutzman, J.M., 1990. High-resolution planktic stable isotope record and spectral analysis for the last 5.35 m.y., Ocean Drilling Program Site 625, Northeast Gulf of Mexico. *Paleoceanography*, 5:507–529.

- Katz, M.E., and Miller, K.G., 1991. Early Paleogene benthic foraminiferal assemblages and stable isotopes in the Southern Ocean. *In* Ciesielski, P.F., Kristoffersen, Y., et al., *Proc. ODP, Sci. Results*, 114: College Station, TX (Ocean Drilling Program), 481–512.
- Kennett, J.P., and Srinivasan, M.S., 1983. *Neogene Planktonic Foraminifera: A Phylogenetic Atlas*: Stroudsburg, PA (Hutchinson Ross).
- Krijgsman, W., Hilgen, F.J., Langereis, C.G., and Zachariasse, W.J., 1994. The age of the Tortonian/Messinian boundary. *Earth Planet. Sci. Lett.*, 121:533–547.
- Kvenvolden, K.A., and McDonald, T.J., 1986. Organic geochemistry on the JOIDES Resolution—an assay. *ODP Tech. Note*, 6.
- Lamont-Doherty Earth Observatory-Borehole Research Group, 1994. *Wireline Logging Services Guide*: Lamont-Doherty Earth Observatory-Borehole Research Group.
- Leckie, R.M., Farnham, C., and Schmidt, M.G., 1993. Oligocene planktonic foraminifer biostratigraphy of Hole 803D (Ontong Java Plateau) and Hole 628A (Little Bahama Bank), and comparison with the southern high latitudes. *In* Berger, W.H., Kroenke, L.W., Mayer, L.A., et al., *Proc. ODP, Sci. Results*, 130: College Station, TX (Ocean Drilling Program), 113–136.
- Li, Q., Radford, S.S., and Banner, F.T., 1992. Distribution of microperforate tenuitellid planktonic foraminifers in Holes 747A and 749B, Kerguelen Plateau. *In* Wise, S.W., Jr., Schlich, R., et al., *Proc. ODP, Sci. Results*, 120: College Station, TX (Ocean Drilling Program), 569–594.
- Loeblich, A.R., Jr., and Tappan, H., 1988. *Foraminiferal Genera and Their Classification*: New York (Van Nostrand Reinhold).
- Lovell, M.A., Harvey, P.K., Brewer, T.S., Williams, C., Jackson, P.D., and Williamson, G., 1998. Application of FMS images in the Ocean Drilling Program: an overview. *In* Cramp, A., MacLeod, C.J., Lee, S.V., and Jones, E.J.W. (Eds.), *Geological Evolution of Ocean Basins: Results from the Ocean Drilling Program*. Geol. Soc. Spec. Publ. London, 131:287–303.
- Lloyd, J., and Moran, K., 1992. ODP GRAPE evaluation: a report to the JOIDES Shipboard Measurements Panel. *Internal Rep., Ocean Drilling Program*.
- Lyle, M., Koizumi, I., Richter, C., et al., 1997. *Proc. ODP, Init. Repts.*, 167: College Station, TX (Ocean Drilling Program).
- Mackensen, A., 1992. Neogene benthic foraminifers from the southern Indian Ocean (Kerguelen Plateau): biostratigraphy and paleoecology. *In* Wise, S.W., Jr., Schlich, R., et al., *Proc. ODP, Sci. Results*, 120: College Station, TX (Ocean Drilling Program), 649–673.
- Mackensen, A., and Berggren, W.A., 1992. Paleogene benthic foraminifers from the southern Indian Ocean (Kerguelen Plateau): biostratigraphy and paleoecology. *In* Wise, S.W., Jr., Schlich, R., et al., *Proc. ODP, Sci. Results*, 120: College Station, TX (Ocean Drilling Program), 603–630.
- Manheim, F.T., and Sayles, F.L., 1974. Composition and origin of interstitial waters of marine sediments, based on deep sea drill cores. *In* Goldberg, E.D. (Ed.), *The Sea* (Vol. 5): *Marine Chemistry: The Sedimentary Cycle*: New York (Wiley), 527–568.
- Martini, E., 1971. Standard Tertiary and Quaternary calcareous nannoplankton zonation. *In* Farinacci, A. (Ed.), *Proc. 2nd Int. Conf. Planktonic Microfossils Roma*: Rome (Ed. Tecnosci.), 2:739–785.
- Mayer, L.A., 1994. Paleoceanography from a single hole to the ocean basins. *Oceanus*, 36:40–44.
- Mazzullo, J.M., Meyer, A., and Kidd, R.B., 1988. New sediment classification scheme for the Ocean Drilling Program. *In* Mazzullo, J., and Graham, A.G. (Eds.), *Handbook for Shipboard Sedimentologists*. ODP Tech. Note, 8:45–67.
- McKee, E.D., and Weir, G.W., 1953. Terminology for stratification and cross-stratification in sedimentary rocks. *Geol. Soc. Am. Bull.*, 64:381–390.
- Miller, K.G., Feigenson, M.D., Wright, J.D., and Clement, B.M., 1991. Miocene isotope reference section, Deep Sea Drilling Project Site 608: an evaluation of isotope and biostratigraphic resolution. *Paleoceanography*, 6:33–52.



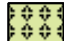







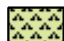



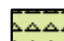


- Miller, K.G., and Katz, M.E., 1987. Oligocene to Miocene benthic foraminiferal and abyssal circulation changes in the North Atlantic. *Micropaleontology*, 33:97–149.
- Miller, K.G., Thompson, P.R., and Kent, D.V., 1993. Integrated late Eocene-Oligocene stratigraphy of the Alabama coastal plain: correlation of hiatuses and stratal surfaces to glacioeustatic lowerings. *Paleoceanography*, 8:313–331.
- Miller, K.G., Wright, J.D., Van Fossen, M.C., and Kent, D.V., 1994. Miocene stable isotopic stratigraphy and magnetostratigraphy of Buff Bay, Jamaica. *Geol. Soc. Am. Bull.*, 106:1605–1620.
- Monechi, S., and Thierstein, H.R., 1985. Late Cretaceous-Eocene nannofossil and magnetostratigraphic correlations near Gubbio, Italy. *Mar. Micropaleontol.*, 9:419–440.
- Montanari, A., Deino, A., Coccioni, R., Langenheim, V.E., Capo, R., and Monechi, S., 1991. Geochronology, Sr isotope analysis, magnetostratigraphy, and planktonic stratigraphy across the Oligocene-Miocene boundary in the Contessa section (Gubbio, Italy). *Newsl. Stratigr.*, 23:151–180.
- Munsell Color Company, Inc., 1994. *Munsell Soil Color Chart*: (Revised ed.): Newburgh, MD (Munsell Color).
- Nocchi, M., Parisi, G., Monaco, P., Monechi, S., Madile, M., Napoleone, G., Ripepe, M., Orlando, M., Premoli Silva, I., and Bice, D.M., 1986. The Eocene-Oligocene boundary in the Umbrian pelagic sequences. In Pomerol, C., and Premoli Silva, I. (Eds.), *Terminal Eocene Events*: New York (Elsevier), Devl. in Paleontol. and Stratigr., 9:25–40.
- Norris, R.D., Kroon, D., Klaus, A., et al., 1998. *Proc. ODP, Init. Repts.*, 171B: College Station, TX (Ocean Drilling Program).
- Okada, H., and Bukry, D., 1980. Supplementary modification and introduction of code numbers to the low-latitude coccolith biostratigraphic zonation (Bukry, 1973; 1975). *Mar. Micropaleontol.*, 5:321–325.
- Perch-Nielsen, K., 1985. Cenozoic calcareous nannofossils. In Bolli, H.M., Saunders, J.B., and Perch-Nielsen, K. (Eds.), *Plankton Stratigraphy*: Cambridge (Cambridge Univ. Press), 427–554.
- Premoli Silva, I., Orlando, M., Monechi, S., Madile, M., Napoleone, G., and Ripepe, M., 1988. Calcareous plankton biostratigraphy and magnetostratigraphy at the Eocene-Oligocene transition in the Gubbio area. In Premoli Silva, I., Coccioni, R., and Montanari, A., *Int. Subcomm. Paleog. Strat., Eocene/Oligocene Meeting, Ancona, Oct. 1987 Spec. Publ.*, II, 6:137–161.
- Pujol, C., and Duprat, J., 1983. Quaternary planktonic foraminifers of the southwestern Atlantic (Rio Grande Rise) Deep Sea Drilling Project Leg 72. In Barker, P.F., Carlson, R.L., Johnson, D.A., et al., *Init. Repts. DSDP, 72*: Washington (U.S. Govt. Printing Office), 601–615.
- Raffi, I., and Flores, J.-A., 1995. Pleistocene through Miocene calcareous nannofossils from eastern equatorial Pacific Ocean. In Pisias, N.G., Mayer, L.A., Janecek, T.R., Palmer-Julson, A., and van Andel, T.H. (Eds.), *Proc. ODP, Sci. Results*, 138: College Station, TX (Ocean Drilling Program), 233–286.
- Rider, M., 1996. *The Geological Interpretation of Well Logs* (2nd ed.): Caithness (Whittles Publishing).
- Schlumberger, 1989. *Log Interpretation Principles/Applications*: Houston, TX (Schlumberger Educ. Services).
- , 1994a. *Geological High-Resolution Magnetic Tool (GHMT) Interpretation Method*: (Schlumberger Riboud Product Center).
- , 1994b. *IPL Integrated Porosity Lithology* (Schlumberger Wireline and Testing), SMP-9270.
- , 1995. *DSI—Dipole Sonic Imager*: (Schlumberger Wireline and Testing), SMP-5128.
- Serra, O., 1984. *Fundamentals of Well-Log Interpretation* (Vol. 1): *The Acquisition of Logging Data*: Dev. Pet. Sci., 15A: Amsterdam (Elsevier).

- , 1986. *Fundamentals of Well-Log Interpretation* (Vol. 2): *The Interpretation of Logging Data*. Dev. Pet. Sci., 15B.
- , 1989. *Formation MicroScanner Image Interpretation*: Houston (Schlumberger Educ. Services), SMP-7028.
- Shafik, S., Watkins, D.K., and Shin, I.C., 1998. Upper Cenozoic calcareous nannofossil biostratigraphy, Côte d'Ivoire-Ghana Margin, eastern equatorial Atlantic. In Mascle, J., Lohmann, G.P., and Moullade, M. (Eds.), *Proc. ODP, Sci. Results*, 159: College Station, TX (Ocean Drilling Program), 509–523.
- Shepard, F., 1954. Nomenclature based on sand-silt-clay ratios. *J. Sediment. Petrol.*, 24:151–158.
- Shipboard Scientific Party, 1992. Explanatory notes. In Davis, E.E., Mottl, M.J., Fisher, A.T., et al., *Proc. ODP, Init. Repts.*, 139: College Station, TX (Ocean Drilling Program), 55–97.
- , 1994. Explanatory notes. In Mountain, G.S., Miller, K.G., Blum, P., et al., *Proc. ODP, Init. Repts.*, 150: College Station, TX (Ocean Drilling Program), 21–42.
- , 1997. Explanatory notes. In Eberli, G.P., Swart, P.K., Malone, M.J., et al., *Proc. ODP, Init. Repts.*, 166: College Station, TX (Ocean Drilling Program), 43–65.
- Sigurdsson, H., Leckie, R.M., Acton, G.D., et al., 1997. *Proc. ODP, Init. Repts.*, 165: College Station, TX (Ocean Drilling Program).
- Spiegler, D., and Jansen, E., 1989. Planktonic foraminifer biostratigraphy of Norwegian Sea sediments: ODP Leg 104. In Eldholm, O., Thiede, J., Taylor, E., et al., *Proc. ODP, Sci. Results*, 104: College Station, TX (Ocean Drilling Program), 681–696.
- Srinivasan, M.S., and Sinha, D.K., 1992. Late Neogene planktonic foraminiferal events of the southwest Pacific and Indian Ocean: a comparison. In Tsuchi, R., and Ingle, Jr., J.C. (Eds.), *Pacific Neogene: Environment, Evolution and Events*: Tokyo (Univ. Tokyo Press), 203–220.
- Stott, L.D., and Kennett, J.P., 1990. Antarctic Paleogene planktonic foraminifer biostratigraphy: ODP Leg 113, Sites 689 and 690. In Barker, P.F., Kennett, J.P., et al., *Proc. ODP, Sci. Results*, 113: College Station, TX (Ocean Drilling Program), 549–569.
- Thomas, E., 1990. Late Cretaceous through Neogene deep-sea benthic foraminifers (Maud Rise, Weddell Sea, Antarctica). In Barker, P.F., Kennett, J.P., et al., *Proc. ODP, Sci. Results*, 113: College Station, TX (Ocean Drilling Program), 571–594.
- Timur, A., and Toksöz, M.N., 1985. Downhole geophysical logging. *Annu. Rev. Earth Planet. Sci.*, 13:315–344.
- Toumarkine, M., and Luterbacher, H., 1985. Paleocene and Eocene planktic foraminifera. In Bolli, H.M., Saunders, J.B., and Perch-Nielsen, K. (Eds.), *Plankton Stratigraphy*: Cambridge (Cambridge Univ. Press), 87–154.
- van Morkhoven, F.P.C.M., Berggren, W.A., and Edwards, A.S., 1986. Cenozoic cosmopolitan deep-water benthic foraminifera. *Bull. Cent. Rech. Explor.—Prod. Elf-Aquitaine*, Mem. 11.
- Weaver, P.P.E., and Clement, B.M., 1987. Magnetobiostratigraphy of planktonic foraminiferal datums, DSDP Leg 94, North Atlantic. In Ruddiman, W.F., Kidd, R.B., Thomas, E., et al., *Init. Repts. DSDP*, 94: Washington (U.S. Govt. Printing Office), 815–829.
- Wright, J.D., and Miller, K.G., 1992. Miocene stable isotope stratigraphy, Site 747, Kerguelen Plateau. In Wise, S.W., Jr., Schlich, R., et al., *Proc. ODP, Sci. Results*, 120: College Station, TX (Ocean Drilling Program), 855–866.
- Zijderveld, J.D.A., Hilgen, F.J., Langereis, C.G., Verhallen, P.J.J.M., and Zachariasse, W.J., 1991. Integrated magnetostratigraphy and biostratigraphy of the upper Pliocene-lower Pleistocene from the Monte Singa and Crotona areas in Calabria, Italy. *Earth Planet. Sci. Letters*, 107:697–714.
- Wentworth, C.K., 1922. A scale of grade and class terms of clastic sediments. *J. Geol.*, 30:377–392.

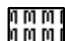
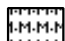
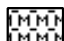
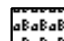
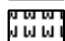
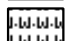
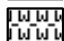
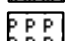
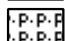
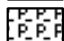
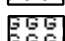

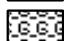

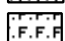
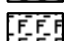
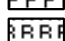
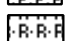
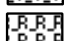
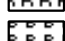
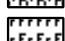
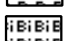
Figure F1. Key to symbols used in core description forms. (Continued on next three pages.)

Lithology

Pelagic Sediment

 Pelagic Limestone	 Nannofossil Ooze	 Diatom-Rad Ooze	 Diatomite
 Foraminiferal Chalk	 Foraminiferal Ooze	 Diatom Ooze	 Radiolarite
 Nanno-Foram Chalk	 Nanno-Foram Ooze	 Radiolarian Ooze	 Spiculite
 Calcareous Chalk	 Calcareous Ooze		 Porcellanite
 Nannofossil Chalk			 Chert

Neritic Sediment

 Mudstone	 Partially Lithified Mudstone	 Unlithified Mudstone	 Bafflestone
 Wackestone	 Partially Lithified Wackestone	 Unlithified Wackestone	
 Packstone	 Partially Lithified Packstone	 Unlithified Packstone	
 Grainstone	 Partially Lithified Grainstone	 Unlithified Grainstone	
 Floatstone	 Partially Lithified Floatstone	 Unlithified Floatstone	
 Rudstone	 Partially Lithified Rudstone	 Unlithified Rudstone	
 Boundstone	 Framestone	 Bindstone	

Siliciclastic Sediments

 Sand or Sandstone	 Silt or Siltstone	 Shale (fissile)	 Breccia
 Silty Sand	 Sandy Silt	 Silty Clay	 Gravel
 Clayey Sand	 Clayey Silt	 Sandy Clay	 Conglomerate
 Sand-Silt-Clay	 Siliceous Clay/Claystone	 Clay or Claystone	 Coal and Peat

Volcaniclastic Sediments



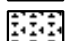

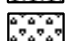
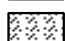














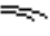
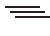
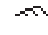









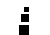





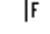




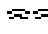

 Volcanic Ash or Tuff	 Volcaniclastic Sand
 Volcanic Lapilli	 Volcaniclastic Breccia
 Volcanic Breccia	 Volcaniclastic Silt

Figure F1 (continued).











Contacts

 Sharp	 Scoured	 Bioturbated	 Uncertain
 Undulating	 Faulted	 Inclined	 Stylolite
 Firmground	 Hardground		



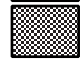
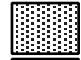

Sedimentary Structures

 Climbing Ripple	 High Angle Tabular Bedding	 Planar Lamination
 Cross Lamination	 Hummocky Cross-strat.	 Planar Tabular Bedding
 Current Ripple	 Imbrication	 Reactivation Surface
 Flaser Bedding	 Low Angle Tabular Bedding	 Trough Cross-strat.
 Herringbone Cross-strat.	 Oscillatory Ripple	 Wavy Parallel Bedding
 Chaotic Bedding	 Graded Bedding	 Reverse Graded Bedding
 Convolute Bedding	 Lenticular Bedding	 Slump
 Coarsening-upward	 Fining Upward	 Cone in Cone Structure
 Birdseye Structure, Keystone Vug	 Mud Cracks	 Tight Zone
 Double Mud Drapes	 Synaeresis Cracks	

Core Disturbance

 Slightly Disturbed	 Biscuit	 Slightly Fractured
 Moderately Disturbed	 Gas Expansion	 Moderately Fractured
 Very Disturbed		 Highly Fragmented
 Soupy		 Breccia

Bioturbation

 Abundant
 Common
 Moderate
 Rare
 Barren

Consolidation (Lithification)



















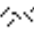






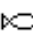
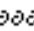




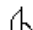




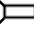















 Lithified
 Partially Lithified
 Unlithified

Figure F1 (continued).

Fossils

 - Algae (undifferentiated)	 - Chara	 - Hydrozoan
 - Algal Stromatolite	 - Coral (azooxanthellate)	 - Mollusc (undifferentiated)
 - Belemnite	 - Coral (colonial)	 - Ostracod
 - Bivalve	 - Coral (solitary)	 - Plant Remain
 - Brachiopod	 - Crinoid	 - Pteropod
 - Bryozoa (articulated branch)	 - Diatoms	 - Scolecodont
 - Bryozoa (articulated zooidal)	 - Echinoderm	 - Serpulid
 - Bryozoa (delicate branching)	 - Fish Remain	 - Shell Fragment
 - Bryozoa (encrusting)	 - Fish Scale	 - Spicule
 - Bryozoa (fenestrate)	 - Fossil ghost	 - Spine
 - Bryozoa (flat robust branching)	 - Fossil fragment	 - Sponge
 - Bryozoa (foliose)	 - Foraminifer (large benthic)	 - Spore, Pollen
 - Bryozoa (nodular/arborescent)	 - Foraminifer (planktonic)	 - Radiolarian
 - Bryozoa (tube-like)	 - Foraminifer (small benthic)	 - Rhodolith
 - Bryozoa (vagrant)	 - Foraminifer (undifferentiated)	 - Rudist (undifferentiated)
 - Calcsphere	 - Gastropod	 - Vertebrate
 - Cephalopod		

Ichnofossils




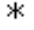






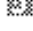
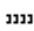















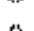




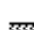
 - Arenicolites	 - Undefined Burrow	 - Rosselia
 - Asterosoma	 - Gyrolithes	 - Schaubcylindrichnus
 - Bergaueria	 - Helminthopsis	 - Skolithos
 - Bored Hardground	 - Macaronichnus	 - Taenidium
 - Chondrites	 - Monocraterion	 - Teichichnus
 - Conichnus	 - Ophiomorpha	 - Terebellina
 - Conostichus	 - Palaeophycus	 - Teredolites
 - Cylindrichnus	 - Planolites	 - Thalassinoides
 - Diplocraterion	 - Pylonichnus	 - Trichichnus
 - Escape Trace	 - Rhizocorallium	 - Trypanites
 - Gastrochaenolites	 - Rootlets	 - Zoophycos

Figure F1 (continued).

Lithologic Accessories

















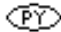

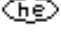
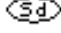



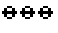
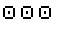







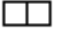


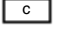



 - Anhydrite	 - Coal Lamina	 - Shale Lamina
 - Ash Layer	 - Dolomitic	 - Silt Lamina
 - Breccia Horizon	 - Organic Shale Lamina	 - Sand Lamina
 - Calcareous	 - Pebbles/Granules	 - Pebbles/Granules/Sand
 - Charcoal Fragments	 - Rip Up Clasts	
 - Calcite Concretion-	 - Ferruginous Concretion	 - Pyrite Concretion
 - Chalcedony/Chert Concretion	 - Hematite Concretion	 - Siderite Concretion
 - Dolomite Concretion	 - Nodule/Concretion, General	
 - Cherty	Kaol - Kaolinitic	Sid - Siderite
Ch - Chlorite	Lth - Lithic	Sm - Smectite
Fld - Feldspathic	Me - Micaceous	S - Sulfur
Fe - Ferruginous	Py - Pyrite	wd - Wood Fragments
Gl - Glauconitic	Q - Quartz Crystals	
 - Coated Grains	 - Oolitic	 - Peloids
 - Fecal Pellets	Palsl - Paleosol Horizon	 - Pisolites
 - Grapestone		
 - Boxwork Structure	 - Clast Imbrication	 - Lithoclast
 - Calcite Cement	 - Crystal Ghost	 - Mottled
 - Cement, General	 - Dropstone	 - Mud Clasts
 - Chalcedony Cement		

Figure F2. The Dunham (1962) classification of limestones according to depositional texture, as modified by Embry and Klovan (1971).

Allochthonous carbonates original components not organically bound during deposition						Autochthonous limestones original components organically bound during deposition		
Less than 10% >2-mm components				Greater than 10% >2-mm components		Boundstone		
Contains lime mud (<0.03 mm)			No lime mud	Matrix supported	>2-mm component supported	By organisms that act as baffles	By organisms that encrust and bind	By organisms that build a rigid framework
Mud supported		Grain supported						
Less than 10% grains (>0.03 mm to <2 mm)	Greater than 10% grains							
Mudstone	Wackestone	Packstone	Grainstone	Floatstone	Rudstone	Bafflestone	Bindstone	Framestone

Figure F3. Udden-Wentworth grain-size classification of terrigenous sediments (from Wentworth, 1922).

Millimeters (mm)	Micrometers (μm)	Phi (ϕ)	Wentworth size class
4096		-12.0	Boulder
256		-8.0	Cobble
64		-6.0	Pebble
4		-2.0	Granule
2.00		-1.0	Very coarse sand
1.00		0.0	Coarse sand
1/2	500	1.0	Medium sand
1/4	250	2.0	Fine sand
1/8	125	3.0	Very fine sand
1/16	63	4.0	Coarse silt
1/32	31	5.0	Medium silt
1/64	15.6	6.0	Fine silt
1/128	7.8	7.0	Very fine silt
1/256	3.9	8.0	Clay
0.00006	0.06	14.0	

Gravel

Sand

Silt

Mud

Figure F4. Diagram showing classification scheme used for siliciclastic sediments and rocks (after Shepard, 1954).

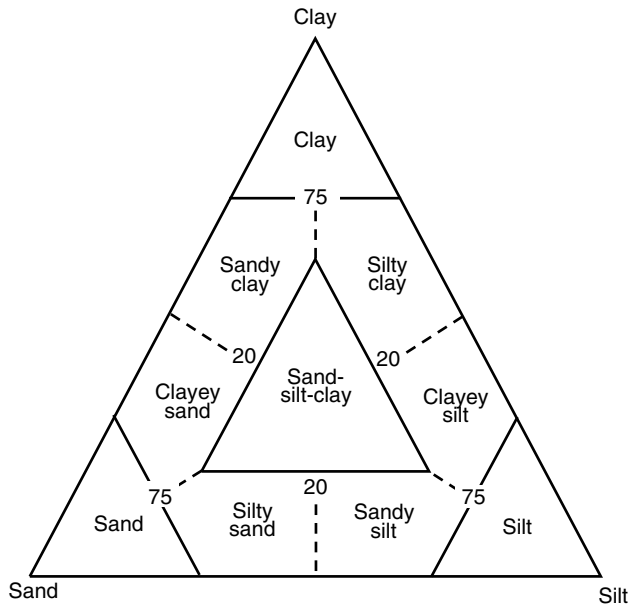


Figure F5. Quaternary through Paleocene chronostratigraphic units correlated with planktonic foraminifer and calcareous nannofossil zonations and with the geomagnetic polarity time scale. Time scales are from Berggren et al. (1995a). Zonations are those of (1) Berggren et al. (1995a), (2) Blow (1969), (3) Jenkins (1985, 1993) (see Fig. F7, p. 52), (4) Martini (1971), and (5) Okada and Bukry (1980). (**Figure shown on next three pages.**)

Figure F5 (continued).

Ma	CHRON	POL.	EPOCH	AGE	BIOZONES																			
					(1)	(3)	(4)	(5)																
20	C6r		Miocene	early	Burdigal.	M2	SN4																	
21	C6An ¹				Aquitanian	M2 (N5)	<i>trilobus</i>			NN2	CN1c													
	C6An ²ⁿ																							
22	C6Ar											M1 (N4)	SN3											
	C6AAr																							
23	C6Bn ¹			SN2 <i>woodi</i>																				
	C6Bn ²ⁿ																							
24	C6Br				SN1 <i>dehisc.</i>					NN1	CN1b CN1a													
	C6Cn ¹																							
C6Cn ²		Oligocene										late	Chatthian	P22	SP15 <i>euaper.</i>		NP25	CP19b						
C6Cr																								
25	C7n ²ⁿ			P21b																				
	C7r																							
26	C7An				P21a	SP14 <i>cubensis</i>				NP24	CP19a													
	C7Ar																							
27	C8n ¹																							
	C8n ²ⁿ																							
28	C8r			P19																				CP17
	C9n																							
29	C9r		P18		SP12 <i>brevis</i>				NP22	CP16c														
	C10n ¹																							
30	C10n ²ⁿ										P17					NP21	CP16a							
	C10r																							
31	C11n ¹			P16														SP11 <i>linaperta</i>				NP19 NP20	CP15b	
	C11n ²ⁿ																							
32	C11r		P15						NP18	CP15a														
	C12n																							
33	C12r										P14	SP10b <i>aculea.</i>				NP17	CP14b							
	C13n																							
34	C13r			P13														SP10a <i>inconsp.</i>						
	C15n																							
35	C15r		P12		SP9 <i>index</i>				NP16	CP14a														
	C16n ¹																							
36	C16n ²ⁿ										P11					NP15c	CP13c							
	C16r																							
37	C17n ¹			P11																		NP15b	CP13b	
	C17n ²																							
38	C17n ³ⁿ		P11																					
	C17r																							
39	C18n ¹										P11													
	C18n ²ⁿ																							
40	C18r			P11																				
	C19n																							
41	C19r		P11																					
	C20n																							
42	C20r										P11													
	C20r																							
43	C20r			P11																				
	C20r																							
44	C20r		P11																					
	C20r																							
45	C20r										P11													
	C20r																							
46	C20r			P11																				
	C20r																							
47	C20r		P11																					
	C20r																							
48	C20r										P11													
	C20r																							
49	C20r			P11																				
	C20r																							
50	C20r		P11																					
	C20r																							
51	C20r										P11													
	C20r																							
52	C20r			P11																				
	C20r																							
53	C20r		P11																					
	C20r																							
54	C20r										P11													
	C20r																							
55	C20r			P11																				
	C20r																							
56	C20r		P11																					
	C20r																							
57	C20r										P11													
	C20r																							
58	C20r			P11																				
	C20r																							
59	C20r		P11																					
	C20r																							
60	C20r										P11													
	C20r																							
61	C20r			P11																				
	C20r																							
62	C20r		P11																					
	C20r																							
63	C20r										P11													
	C20r																							
64	C20r			P11																				
	C20r																							
65	C20r		P11																					
	C20r																							
66	C20r										P11													
	C20r																							
67	C20r			P11																				
	C20r																							
68	C20r		P11																					
	C20r																							
69	C20r										P11													
	C20r																							
70	C20r			P11																				
	C20r																							
71	C20r		P11																					
	C20r																							
72	C20r										P11													
	C20r																							
73	C20r			P11																				
	C20r																							
74	C20r		P11																					
	C20r																							
75	C20r										P11													
	C20r																							
76	C20r			P11																				
	C20r																							
77	C20r		P11																					
	C20r																							
78	C20r										P11													
	C20r																							
79	C20r			P11																				
	C20r																							
80	C20r		P11																					
	C20r																							
81	C20r										P11													
	C20r																							
82	C20r			P11																				
	C20r																							
83	C20r		P11																					
	C20r																							
84	C20r										P11													
	C20r																							
85	C20r			P11																				
	C20r																							
86	C20r		P11																					
	C20r																							
87	C20r										P11													
	C20r																							
88	C20r			P11																				
	C20r																							
89	C20r		P11																					
	C20r																							
90	C20r										P11													
	C20r																							
91	C20r			P11																				
	C20r																							
92	C20r		P11																					
	C20r																							
93	C20r										P11													
	C20r																							
94	C20r			P11																				
	C20r																							
95	C20r		P11																					
	C20r																							
96	C20r										P11													
	C20r																							
97	C20r			P11																				
	C20r																							
98	C20r		P11																					
	C20r																							
99	C20r										P11													
	C20r																							
100	C20r			P11																				
	C20r																							

Figure F5 (continued).

Ma	CHRON	POL.	EPOCH	AGE	BIOZONES						
					(1)	(3)	(4)	(5)			
40			Eocene	middle	Lutetian	P13	SP10a <i>inconsp.</i>	NP17	CP14b		
41	C18r										
	C19n										
42	C19r							P12		NP16	CP14a
43	C20n								SP9 <i>index</i>		
44								NP15c	CP13c		
45	C20r					P11		NP15b	CP13b		
46											
47	C21n							NP15a	CP13a		
48	C21r					P10	SP8b <i>soldado</i>	NP14b	CP12b		
49	C22n		early	Ypresian			NP14a	CP12a			
50	C22r						P9	SP8a <i>primitiva</i>	NP13	CP11	
							P8				
51	C23n ¹ 2n						P7	SP7 <i>crater</i>	NP12	CP10	
52	C23r										
53	C24n ¹ 2 3n						P6b	SP6 <i>wilcox</i>	NP11	CP9b	
54	C24r						P6a	SP5 <i>velasco</i>	NP10	CP9a	

Figure F6. The zonal schemes of Martini (1971) and Bukry and Okada (1980), defining events and their proxies. Proxies are indicated by *.

Series	Epoch	Martini (1971) modified	Bukry and Okada (1980) (Sub)zones	Events defining (sub)zonal boundaries	
Pleistocene	late	NN21	CN15	▲ <i>Emiliana huxleyi</i>	
		NN20	CN14	▼ <i>Pseudoemilinia lacunosa</i>	
	early	NN19		b	▲ <i>Gephyrocapsa oceanica</i>
		CN13	b	▲ <i>Gephyrocapsa caribbeanica</i>	
	a		CN12	▼ <i>Discoaster brouweri</i>	
		▼ <i>Discoaster pentaradiatus</i>			
	Pliocene	late	NN18	CN12	▼ <i>Discoaster surculus</i>
			NN17		c
		early	NN16	b	▼ <i>Discoaster tamalis</i>
			a	CN11	▼ <i>Sphenolithus</i> spp. *
▼ <i>R. pseudoumbilicus</i> (<7 microns)					
b		CN11	▲ <i>Pseudoemiliana lacunosa</i> *		
			▲ <i>Acme D. asymmetricus</i>		
a		CN10	▼ <i>Amaurolithus</i> spp.		
			▲ <i>Ceratolithus rugosus</i>		
Miocene		late	NN14–NN13	CN10	▲ <i>Ceratolithus rugosus</i>
	NN12		b		◆ <i>Ceratolithus armatus</i>
	a	CN9	◆ <i>Triquetrorhabdulus rugosus</i>		
			▼ <i>Discoaster quinqueramus</i>		
	b	CN9	◆ <i>Amaurolithus</i> spp.		
			◆ <i>Minylitha convalis</i> *		
	a	CN9	▲ <i>Discoaster quinqueramus</i>		
			▲ <i>Discoaster berggrenii</i>		
	b	CN8	◆ <i>Discoaster neorectus</i>		
			◆ <i>Discoaster bollii</i> *		
a	CN8	▼ <i>Discoaster hamatus</i>			
		▲ <i>Catinaster calyculus</i>			
b	CN7	▲ <i>Discoaster hamatus</i>			
		▲ <i>Discoaster hamatus</i>			
a	CN6	▲ <i>Catinaster coalitus</i>			
		▲ <i>Discoaster kugleri</i>			
middle	NN7	CN5	▼ <i>Sphenolithus heteromorphus</i>		
	NN6	CN5	▲ <i>Helicosphaera ampliaperta</i>		
early	NN5	CN4	▼ <i>Sphenolithus heteromorphus</i>		
	NN4	CN3	▲ <i>Sphenolithus belemnos</i>		
a	CN2	▲ <i>Triquetrorhabdus carinatus</i>			
		▲ <i>Sphenolithus belemnos</i>			
b	CN1	▲ <i>Orthorhabus serratus</i> *			
		▲ <i>Discoaster druggii</i>			
late Oligo.	a	NN1	CN1	▼ <i>Acme C. abisectus</i>	
		NN25	CP19b	▼ <i>Helicosphaera recta</i>	
				▼ <i>Sphenolithus ciproensis</i>	

Series	Epoch	Martini (1971) (Sub)zones	Bukry and Okada (1980) (Sub)zones	Events used to define (sub)zonal boundaries	
Oligocene	late	NN1	CN1	▼ <i>Acme C. abisectus</i>	
		NP25	CP19	a	▼ <i>Sphenolithus ciproensis</i>
	NP24			b	▼ <i>Sphenolithus distentus</i>
	early	NP23	CP18	a	▲ <i>Sphenolithus ciproensis</i>
				CP17	▲ <i>Sphenolithus distentus</i>
	NP22	CP16	c	▼ <i>R. umbilicus</i>	
			b	▼ <i>Coccolithus formosus</i>	
	a	CP16	b	▼ <i>Acme E. subdisticha</i>	
			a	▼ <i>Discoaster barbadiensis</i>	
	Eocene	late	NP19–20	CP15	▼ <i>Discoaster saipanensis</i>
NP18			b		▲ <i>Isthmolithus recurvus</i>
middle		NP17	CP14	a	◆ <i>Chiasmolithus oamaruensis</i>
				◆ <i>Chiasmolithus grandis</i>	
a		CP14	b	▼ <i>Chiasmolithus solitus</i>	
			a	▼ <i>Blackites gladius</i>	
c		NP15	CP13	c	▼ <i>R. umbilicus</i> (>11 microns)
				b	▼ <i>Chiasmolithus gigas</i>
a		CP13	a	▲ <i>Chiasmolithus gigas</i>	
			b	▲ <i>Nannotetrina fulgens</i>	
early	NP14	CP12	a	▲ <i>Blackites inflatus</i>	
			b	▲ <i>Discoaster subloadoensis</i>	
NP13	CP11	a	▲ <i>Coccolithus crassus</i>		
		b	▲ <i>Tribrachiatus orthostyltus</i>		
NP12	CP10	a	▲ <i>Discoaster lodoensis</i>		
		b	▼ <i>Tribrachiatus contortus</i>		
NP11	CP9	a	▲ <i>Discoaster diastypus</i>		
		b	▲ <i>Rhomboaster cuspis</i>		
NP10	CP8	a	▲ <i>C. eodela</i>		
		b	▲ <i>Discoaster multiradiatus</i>		
late	NP9	CP7	a	▲ <i>Discoaster nobilis</i>	
			b	▲ <i>Heliolithus riedelii</i>	
NP8	CP6	a	▲ <i>Discoaster mohleri</i>		
		b	▲ <i>Heliolithus kleinpellii</i>		
NP7	CP5	a	▲ <i>F. tympaniformis</i>		
		b	▲ <i>Ellipsolithus macellus</i>		
NP6	CP4	a	▲ <i>Chiasmolithus danicus</i>		
		b	▲ <i>Cruciplacolithus tenuis</i>		
NP5	CP3	a			
		b			
NP4	CP2	a			
		b			
early	NP3	CP1	a		
			b		
NP2	CP1	a			
		b			
NP1	CP1	a			

Figure F7. The events that define the zonal scheme of Jenkins (1985, 1993). Ages are from (1) Berggren et al. (1995a) and (2) Chaproniere et al. (1995). Parentheses indicate ages without paleomagnetic control.

Age (Ma)		Zones	Datum Levels
(1)	(2)		
2.0	1.96	SN14 <i>Gr. truncatulinoides</i>	▲ <i>Globorotalia truncatulinoides</i>
	3.2	SN13 <i>Gr. inflata</i>	▲ <i>Globorotalia inflata</i>
	4.5	SN12b <i>Gr. puncticulata</i>	
4.2	5.3	SN12a <i>Gr. pliozea</i>	▼ <i>Globorotalia pliozea</i> ▲ <i>Globorotalia puncticulata</i>
6.8	7.12	SN11 <i>Gr. conomiozea</i>	▲ <i>Globorotalia conomiozea</i>
		SN10 <i>Gr. miotumida</i>	
10.1		SN9 <i>N. continuaosa</i>	▼ <i>Neogloboquadrina continuaosa</i>
		SN8 <i>N. nympa</i>	▼ <i>Neogloboquadrina nympa</i>
11.4	11.4	SN7 <i>P. mayeri</i>	▼ <i>Paragloborotalia mayeri</i>
	12.1	SN6 <i>O. suturalis</i>	▲ <i>Orbulina suturalis</i>
15.1	15.1	SN5 <i>P. glomerosa curva</i>	▲ <i>Praeorbulina glomerosa curva</i>
16.3	16.3	SN4 <i>Gs. trilobus</i>	▲ <i>Globigerinoides trilobus</i>
	18.8	SN3 <i>G. woodi connecta</i>	▲ <i>Globoturborotalita woodi connecta</i>
	20.9	SN2 <i>G. woodi woodi</i>	▲ <i>Globoturborotalita woodi woodi</i>
	22.6	SN1 <i>G. dehiscens</i>	▲ <i>Globoquadrina dehiscens</i>
23.2	23.2	SP15 <i>T. euapertura</i>	
28.5		SP14 <i>C. cubensis</i>	▼ <i>Chiloguembelina cubensis</i>
30.0	30.0	SP13 <i>S. angiporoides</i>	▼ <i>Subbotina angiporoides</i>
	31.5	SP12 <i>S. brevis</i>	▼ <i>Subbotina brevis</i>
	33.4	SP11 <i>S. linaperta</i>	
37.7	36.7	SP10 <i>A. aculeata</i> <i>T. inconspicua</i>	▼ <i>Acarinina aculeata</i> ▲ <i>Chiloguembelina cubensis</i>
	41.2	SP9 <i>G. index</i>	▲ <i>Globigerapsis index</i>
42.9	42.9	SP8 <i>A. primitiva</i>	
50.8	48.8	SP7 <i>M. crater</i>	▼ <i>Morozovella crater</i>
54.0	54.0	SP6 <i>P. wilcoxensis</i>	▲ <i>Pseudohastigerina wilcoxensis</i>
	56.3	SP5 <i>M. velascoensis</i>	▲ <i>Morozovella velascoensis</i>
(60.0)	61.0	SP4 <i>P. pseudomenardii</i>	▲ <i>Planorotalites pseudomenardii</i>
	59.2	SP3 <i>S. triloculinoides</i>	
(64.5)		SP2 <i>G. daubjergensis</i>	▼ <i>Globoconusa daubjergensis</i>
	64.7	SP1 <i>"G." pauciloculata</i>	▼ <i>"Globigerina" pauciloculata</i>

M. formosa

Figure F8. A. A 50-m interval of color reflectance records from Holes 1126B (solid line) and 1126C (dashed line) on the meters below seafloor (mbsf) scale. Records from different holes are offset for convenience. Equivalent events in adjacent holes are not aligned. B. Example of the composite section for the same interval shown in A. Events are now aligned on the meters composite depth (mcd) scale. C. The spliced record from the same site as above.

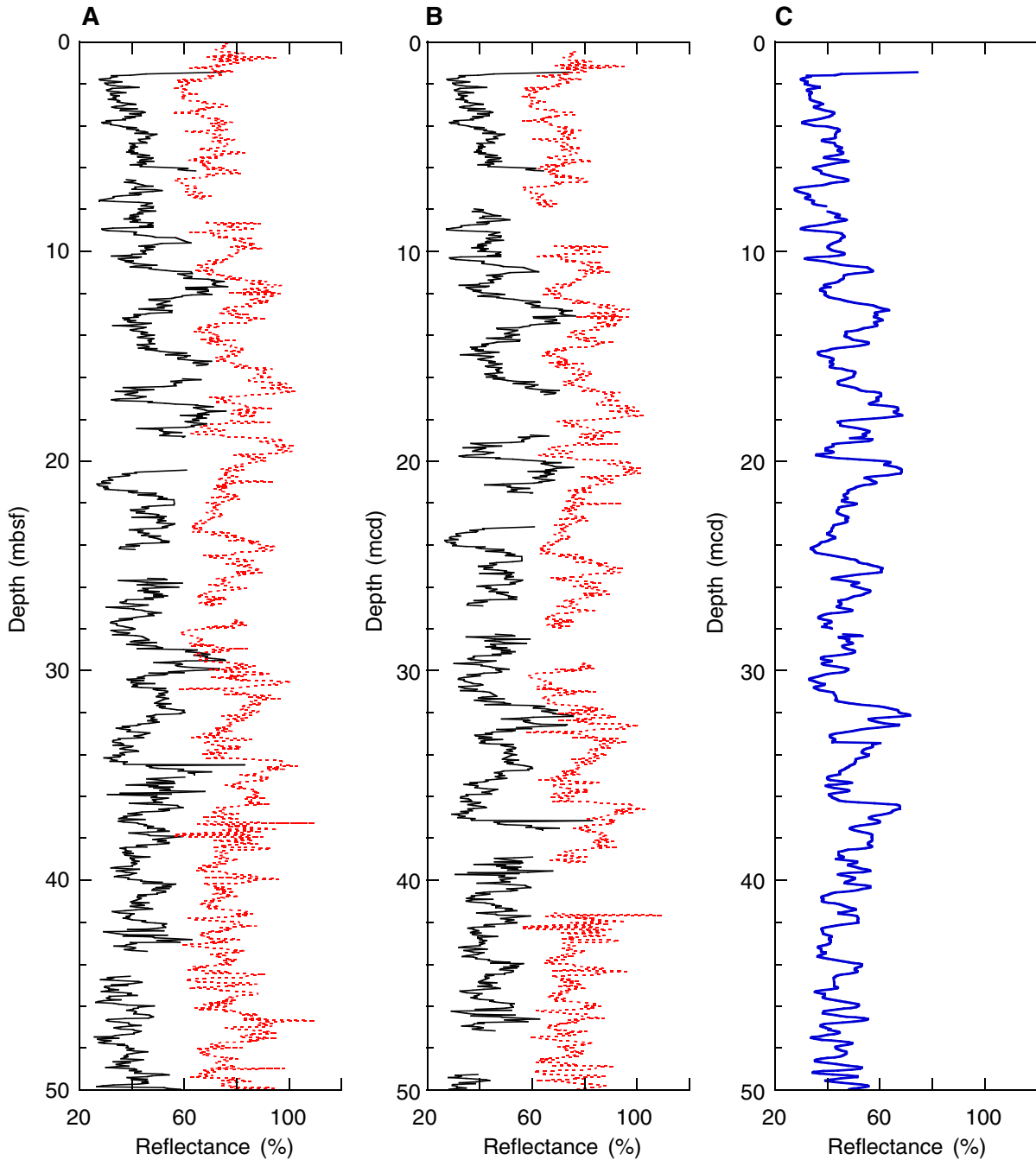


Figure F9. Flow chart depicting the sequence of physical properties measurements for unconsolidated, semilithified, and consolidated sediment cores analyzed during Leg 182.

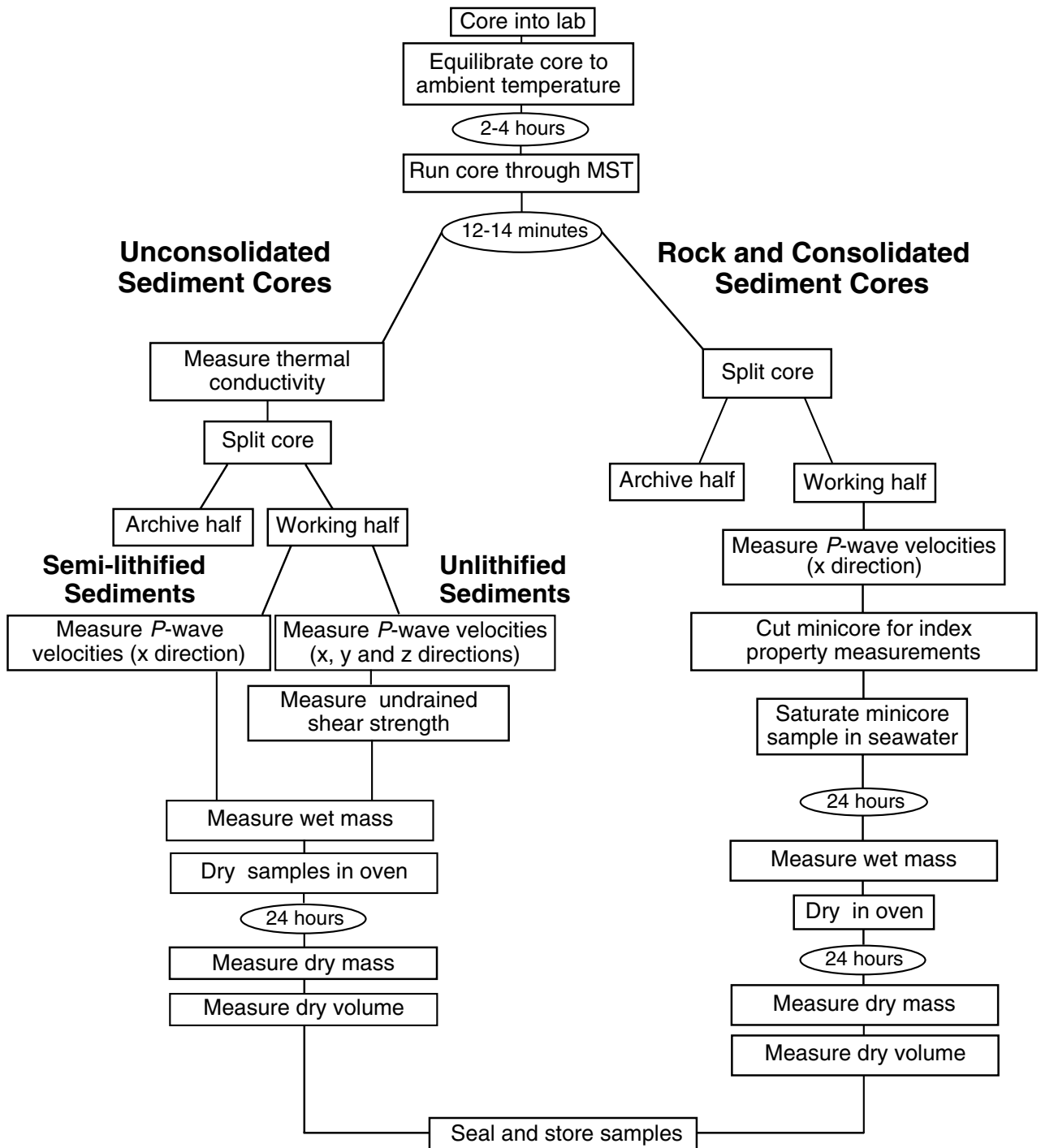


Figure F10. Schematic illustration of the configurations of tool strings run during Leg 182. Abbreviations as in Tables T8, p. 70, and T9, p. 71.

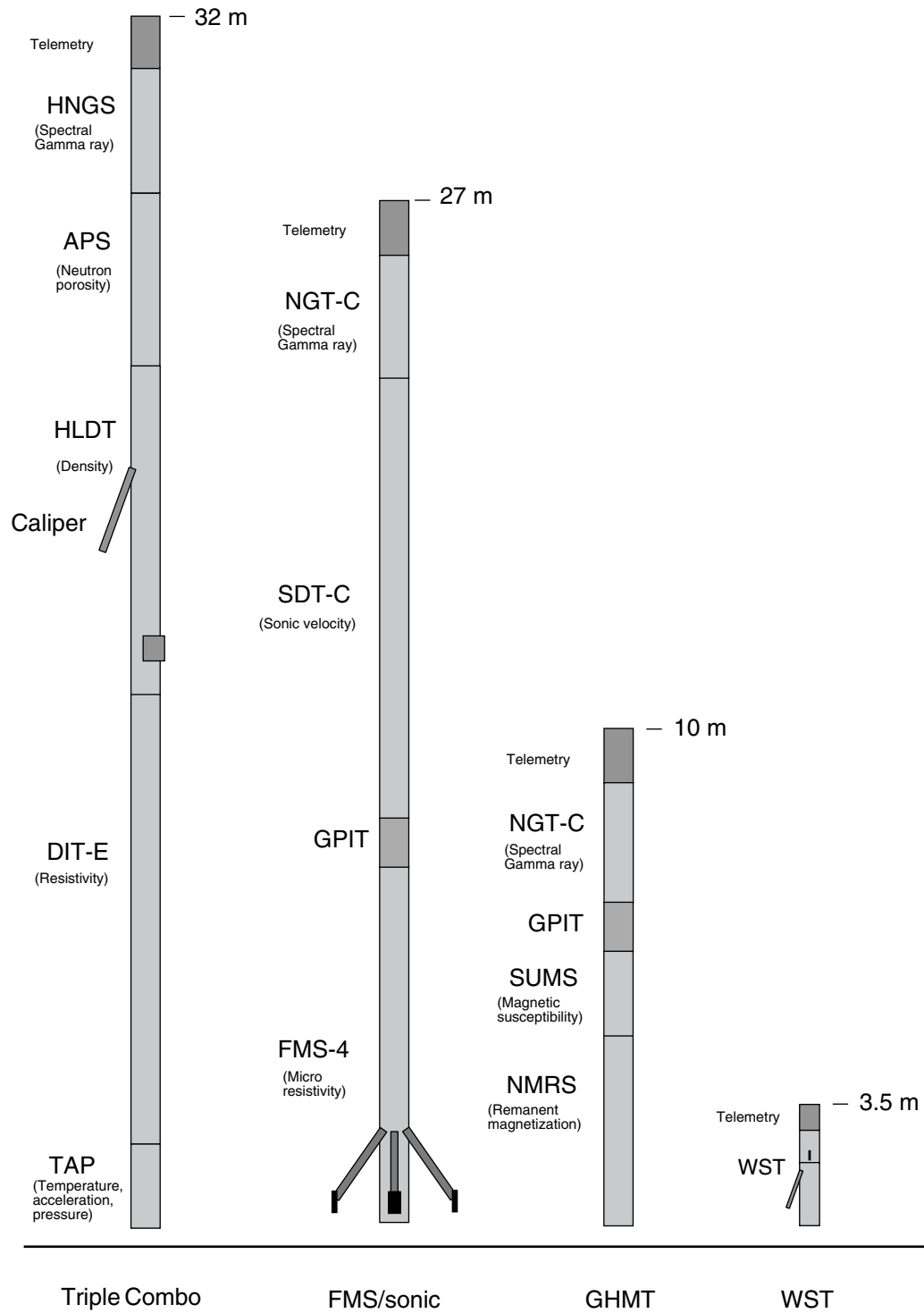


Figure F11. Map of the western Great Australian Bight showing Leg 182 drill sites relative to the Japan National Oil Corporation (JNOC, 1990) seismic grid (heavy lines), together with reprocessed Esso (1979) seismic lines over the Eyre Terrace (lighter dashed lines). The location of exploration drillhole Jerboa-1 is also shown.

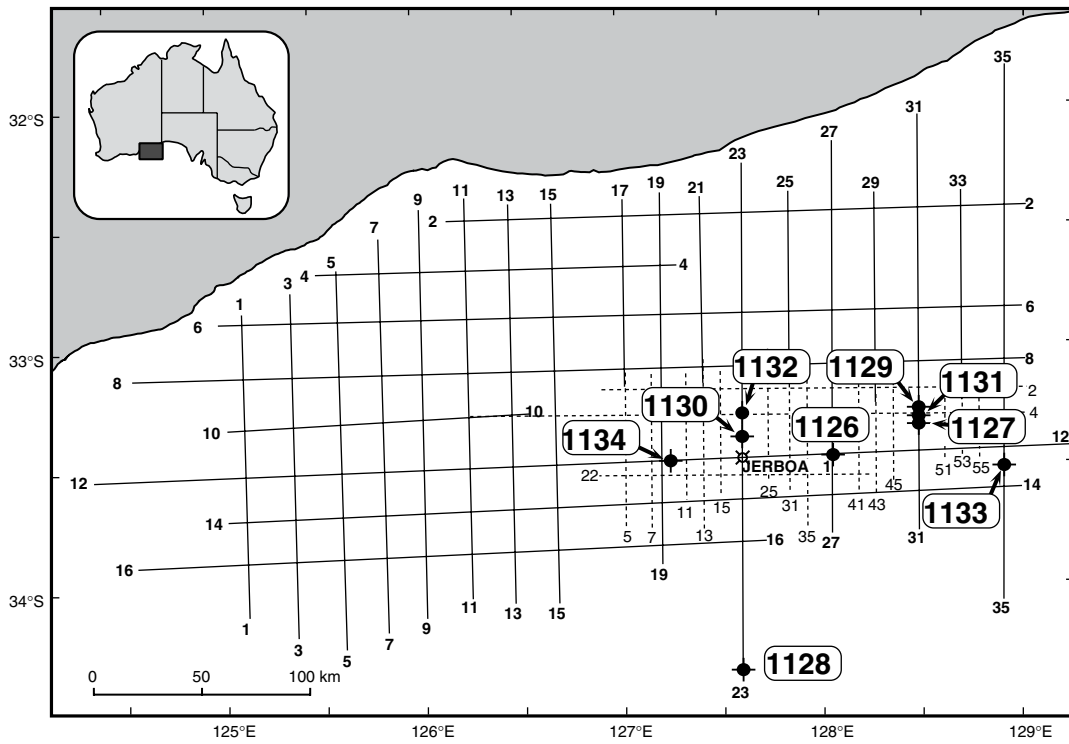


Figure F12. Map showing Leg 182 drill sites relative to the Australian Geological Survey Organisation (AGSO, 1996) high-resolution site-survey seismic grid (AGSO169).

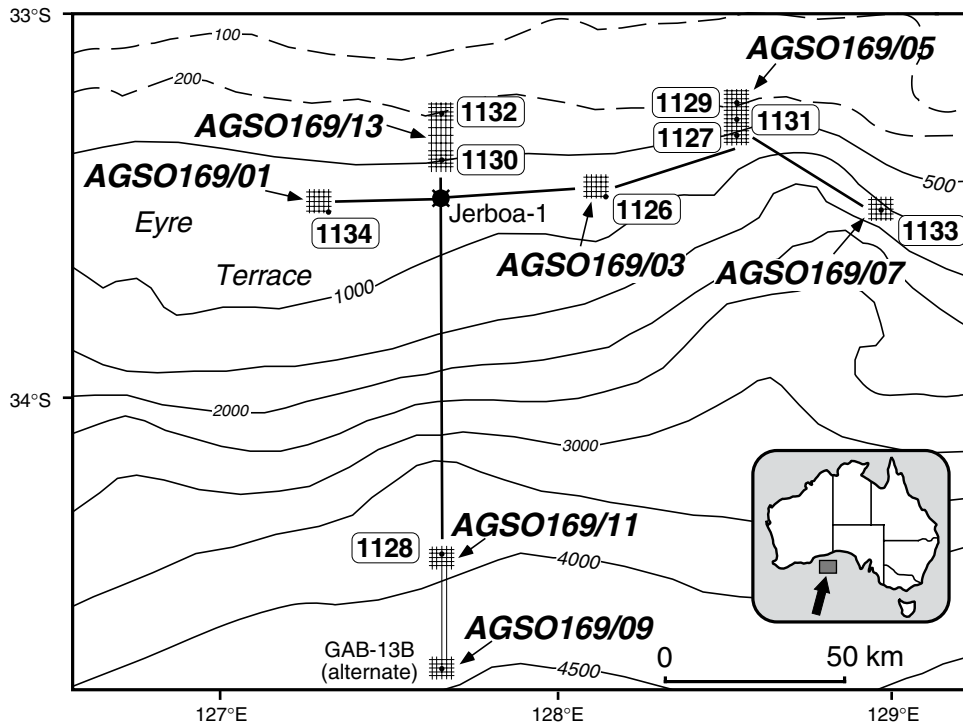


Table T1. Lithologic description of granular sediments.

Sediment class	Major modifiers	Principal names	Minor modifiers
Pelagic sediment	<ol style="list-style-type: none"> 1. Composition of pelagic grains present in major amounts 2. Texture of clastic grains present in major amounts 	<ol style="list-style-type: none"> 1. Ooze 2. Chalk 3. Pelagic limestone 4. Radiolarite 5. Diatomite 6. Spicule 7. Porcellanite 8. Chert 	<ol style="list-style-type: none"> 1. Composition of pelagic and neritic grains present in minor amounts 2. Texture of clastic grains present in minor amounts
Siliciclastic sediment	<ol style="list-style-type: none"> 1. Composition of all grains present in major amounts 2. Grain fabric (gravels only) 3. Grain shape (optional) 4. Sediment color (optional) 	<ol style="list-style-type: none"> 1. Gravel 2. Sand 3. Silt 4. Clay, etc. 	<ol style="list-style-type: none"> 1. Composition of all grains present in minor amounts 2. Texture and composition of siliciclastic grains present as matrix (for coarse-grained clastic sediments)
Volcaniclastic sediment	<ol style="list-style-type: none"> 1. Composition of all volcaniclasts present in major amounts 2. Composition of all pelagic and neritic grains 3. Texture of siliciclastic grains present in major amounts 	<ol style="list-style-type: none"> 1. Breccia 2. Lapilli 3. Ash/tuff 4. Volcanic, etc. 	<ol style="list-style-type: none"> 1. Composition of all volcaniclastics present in minor amounts 2. Composition of all neritic and pelagic grains present in minor amounts 3. Texture of siliciclastic grains present in minor amounts

Table T2. Lithologic description of nonpelagic calcareous sediments and rocks, including the major modifiers.

Sediment class	Major modifiers	Names
Nonpelagic sediment	<ol style="list-style-type: none"> 1. Texture 2. Hydrodynamically accumulated or primary biogenic in situ formation 3. Degree of lithification 	<ol style="list-style-type: none"> 1. Mudstone, partially lithified mudstone, unlithified mudstone 2. Wackestone, partially lithified wackestone, unlithified wackestone 3. Packstone, partially lithified packstone, unlithified packstone 4. Grainstone, partially lithified grainstone, unlithified grainstone 5. Floatstone, partially lithified floatstone, unlithified floatstone 6. Rudstone, partially lithified rudstone, unlithified rudstone

Table T3. Ages of calcareous nannofossil datum levels used on Leg 182. (See table notes. Continued on next three pages.)

Event	Zone (Base)	Age (Ma)	Reference
B Acme <i>Emiliana huxleyi</i>		0.085	2
B <i>Emiliana huxleyi</i>	CN15	0.248	2
T <i>Pseudoemiliana lacunosa</i>	CN14b	0.408	2
B <i>Gephyrocapsa parallela</i>		0.94	2
Reentrance <i>Gephyrocapsa</i> spp. (medium)	CN14a?	0.97	2
T <i>Gephyrocapsa</i> spp. (large)		1.18	2
B <i>Gephyrocapsa</i> spp. (large)		1.40	2
T <i>Helicosphaera sellii</i>		1.41	2
T <i>Calcidiscus macintyreii</i>		1.65	2
B <i>Gephyrocapsa caribbeanica</i>	CN13b?	1.71	2
Pleistocene/Pliocene boundary		1.71	
T <i>Discoaster brouweri</i>	CN13a	1.95	2
B Acme <i>Discoaster triradiatus</i>		2.00	2
T <i>Discoaster pentaradiatus</i>	CN12d	2.36	2
T <i>Discoaster surculus</i>	CN12c	2.51	2
T <i>Discoaster tamalis</i>	CN12b	2.82	2
T <i>Sphenolithus</i> spp.	CN12a	3.62	2
T <i>Reticulofenestra pseudoumbilicus</i>	CN12a	3.83	2
T <i>Amaurolithus</i> spp.	CN11	4.50	2
T <i>Ceratolithus acutus</i>		5.04	3
B <i>Ceratolithus rugosus</i>	CN10c	5.05	2
B <i>Ceratolithus acutus</i>	CN10b	5.09	2
T <i>Triquetrorhabdulus rugosus</i>		5.23	2
Pliocene/Miocene boundary		5.30	
T <i>Discoaster quinqueramus</i>	CN10a	5.6	1
T <i>Amaurolithus amplificus</i>		5.9	1
B <i>Amaurolithus amplificus</i>		6.6	1
T Paracme <i>R. pseudoumbilicus</i>		6.8	4
B <i>Amaurolithus primus</i>	CN9b	7.2	1
T <i>Discoaster loeblichii</i>		7.4	1
T <i>Minylitha convalis</i>		7.8	1
B <i>Discoaster berggrenii</i>	CN9a	8.6	1
B <i>Discoaster loeblichii</i>		8.7	1
B Paracme <i>R. pseudoumbilicus</i>		8.8	4
T <i>Discoaster bollii</i>		9.1	1
T <i>Catinaster calyculus</i>		9.36	3
T <i>Discoaster hamatus</i>	CN8a	9.4	1
B <i>Minylitha convallis</i>		9.5	1
B <i>Discoaster neohamatus</i>		9.6	4
B <i>Discoaster hamatus</i>	CN7	10.7	1
T <i>Coccolithus miopelagicus</i>		11.0	3
B <i>Catinaster coalitus</i>	CN6	11.3	1
T <i>Discoaster kugleri</i>		11.5	1
B <i>Discoaster kugleri</i>		11.8	1
T <i>Coronocyclus nitescens</i>		12.1	4
B <i>Calcidiscus macintyreii</i> >11µm		12.3	4
B <i>Triquetrorhabdulus rugosus</i>		13.2	1
T <i>Calcidiscus premacintyreii</i>		12.7	4
T <i>Discoaster signus</i>		12.7	4
Tc <i>Cyclicargolithus floridanus</i>		13.2	4
T <i>Sphenolithus heteromorphus</i>	CN5a	13.6	1
T <i>Helicosphaera ampliapertura</i>	CN4	15.6	1
B <i>Discoaster signus</i>		16.2	4
T Abundant <i>Discoaster deflandrei</i>		16.2	4
B <i>Calcidiscus premacintyreii</i>		17.4	5
B <i>Sphenolithus heteromorphus</i>	CN3	18.2	1
T <i>Sphenolithus belemnus</i>		18.3	1
B <i>Sphenolithus belemnus</i>	CN2	19.2	1
T <i>Triquetrorhabdulus carinatus</i>		23.1	1
T <i>Triquetrorhabdulus serratus</i>		23.2	1
T <i>Sphenolithus umbrellus</i>		23.6	1
T <i>Sphenolithus capricornutus</i>		23.7	1
B <i>Discoaster druggi</i>	CN1c	23.3	6
T <i>Sphenolithus delphix</i>		23.8	1

Table T3 (continued).

Event	Zone (Base)	Age (Ma)	Reference
Miocene/Oligocene boundary		23.8	
T <i>Dictyococcites bisectus</i>	CN1c	23.9	1
B <i>Sphenolithus delphix</i>		24.3	1
T <i>Zygrhablithus bijugatus</i>		24.5	1
T <i>Sphenolithus ciproensis</i>	CN1a	24.75	1
T <i>Sphenolithus distentus</i>	CP19b	27.5	1
T <i>Sphenolithus predistentus</i>		27.5	1
T <i>Sphenolithus pseudoradians</i>		29.1	1
B <i>Sphenolithus ciproensis</i>	CP19a	29.9	1
B <i>Sphenolithus distentus</i>	CP18	31.5-33.1	1
T <i>Reticulofenestra umbilicus</i>	CP17	32.3	1
T <i>Coccolithus formosus</i>	CP16c	32.8	1
T <i>Chiasmolithus oamaruensis</i>		33.7	1
Oligocene/Eocene boundary		33.7	
T <i>Discoaster saipanensis</i>	CP16a	34.2	1
T <i>Discoaster barbadiensis</i>	CP16a	34.3	1
T <i>Cribracentrum reticulatum</i>		35.0	1
B <i>Isthmolithus recurvus</i>		36.0	1
T <i>Calcidiscus protoannulus</i>		36.8	7
B <i>Chiasmolithus oamaruensis</i>	CP15	37.0	1
T <i>Chiasmolithus grandis</i>	CP15	37.1	1
B <i>Dictyococcites bisecta</i>		38.0	1
T <i>Chiasmolithus solitus</i>	CP14b	40.4	1
B <i>Dictyococcites hesslandii</i>		41.8	7
T <i>Nannotetrina fulgens</i>		43.1	1
T <i>Blackites gladius</i>		43.4	1
B <i>Reticulofenestra umbilicus</i>	CP14a	43.7	1
T <i>Chiasmolithus gigas</i>	CP13c	44.5	1
B <i>Chiasmolithus gigas</i>	CP13b	46.1	1
B <i>Nannotetrina fulgens</i>	CP13a	47.3	1
T <i>Discoaster lodoensis</i>		47.9	1
B <i>Rhabdosphaera inflata</i>		48.5	1
B <i>Nannotetrina</i> spp.		49.2	8
B <i>Discoaster subloadoensis</i>	CP12	49.7	1
T <i>Tribrahiatus orthostylus</i>		50.6	1
B <i>Discoaster lodoensis</i>	CP10	52.85	1
T <i>Sphenolithus radians</i>		53.1	1
T <i>Tibrahiatus contortus</i>		53.6	1
B <i>Tibrahiatus orthostylus</i>		53.6	1
B <i>Discoaster diastypus</i>	CP9a	53.9	8
T <i>Ericsonia robusta</i>		54.0	8
B <i>Tibrahiatus contortus</i>	CP9a	54.3	1
Eocene/Paleocene boundary		54.5	
B <i>Tibrahiatus (Rhomboaster) bramlettei</i>		55.0	8
B <i>Rhomboaster</i> spp.		55.1	8
T <i>Fasciculithus tympaniformis</i>		55.33	1
B <i>Camplyosphaera eodela</i>	CP8b	55.5	1
B <i>Discoaster multiradiatus</i>	CP8a	56.2	1
B <i>Discoaster okadai</i>		56.8	1
B <i>Discoaster nobilis</i>	CP7	56.9	1
B <i>Heliolithus riedelii</i>		57.3	1
T <i>Heliolithus kleinpellii</i>		56.6	8
B <i>Discoaster mohlerii</i>	CP6	57.5	1
B <i>Sphenolithus anarrhopus</i>		58.4	1
T <i>Chiasmolithus danicus</i>		57.5	9
B <i>Heliolithus kleinpellii</i>	CP5	58.4	1
B <i>Heliolithus cantabriae</i>		58.2	8
T <i>Fasciculithus pileatus</i>		58.6	8
T <i>Cruciplacolithus tenuis</i>		58.6	9
B <i>Fasciculithus</i> spp.		59.2	8
B <i>Sphenolithus primus</i>		60.6	1
B <i>Chiasmolithus bidens</i>		60.7	1
B <i>Ellipsolithus macellus</i>	CP3	62.2	1
B <i>Chiasmolithus danicus</i>	CP2	63.8	1
B <i>Cruciplacolithus tenuis</i>	CP1b	64.5	1
B <i>Cruciplacolithus primus</i>		64.8	1

Table T3 (continued).

Event	Zone (Base)	Age (Ma)	Reference
B <i>Biantholithus sparsus</i>		65.0	1
T Cretaceous taxa	CP1a	65.0	1
Tertiary/Cretaceous boundary		65.0	
B <i>Micula prinsii</i>		66.0	10
B <i>Nephrolithus frequens</i> (low latitude)		67.2	10
B <i>Micula murus</i>		68.5	10
T <i>Reinhardtites levis</i>		69.4	10
T <i>Quadrum trifidum</i>		71.3	10
Maastrichtian/Campanian boundary		71.3	
T <i>Tranolithus phacelosus</i>		71.6	10
T <i>Aspidolithus parvus</i>		74.6	10
T <i>Eiffelithus eximius</i>		75.3	10
T <i>Lithastrinus grillii</i>		75.1	10
B <i>Quadrum trifidum</i>		76.1	10
B <i>Quadrum sissinghii</i>		77.1	10
B <i>Ceratolithoides aculeus</i>		78.5	10
T <i>Bukryaster hayii</i>		79.8	10
T <i>Marthasterites furcatus</i>		80.6	10
B <i>Ceratolithoides verbeekii</i>		82.0	10
B <i>Aspidolithus parvus constrictus</i>		83.5	10
Campanian/Santonian boundary		83.5	
B <i>Calculites obscurus</i>		83.8	10
B <i>Lucianorhabdus cayeuxii</i>		84.8	10
T <i>Lithastrinus septenarius</i>		84.9	10
B <i>Lithastrinus grillii</i>		85.8	10
Santonian/Coniacian boundary		85.8	
B <i>Reinhardtites anthophorus</i>		85.8	10
B <i>Micula decussata</i>		87.2	10
Coniacian/Turonian boundary		89.0	
B <i>Marthasterites furcatus</i>		89.3	10
B <i>Lucianorhabdus maleformis</i>		91.0	10
B <i>Eiffelithus eximius</i>		91.0	10
B <i>Quadrum gartnerii</i>		93.5	10
Cenomanian/Turonian boundary		93.5	
T <i>Corollithion kennedyi</i>		93.9	10
T <i>Rhagodiscus asper</i>		93.9	10
T <i>Axopodorhabdus albianus</i>		93.9	10
T <i>Microstaurus chastiatus</i>		94.4	10
B <i>Microrhabdulus decoratus</i>		95.2	10
B <i>Lithraphidites acutus</i>		95.2	10
B <i>Corollithion kennedyi</i>		97.4	10
Albian/Cenomanian boundary		98.9	
T <i>Hayesites albiensis</i>		99.0	10
T <i>Rucinolithus irregularis</i>		99.0	10
B <i>Eiffelithus turriseiffelii</i>		101.7	10
B <i>Eiffelithus</i> spp. (small)		103.8	10
B <i>Axopodorhabdus albianus</i>		106.5	10
B <i>Tranolithus phacelosus</i>		106.5	10
B <i>Cribrosphaerella ehrenbergii</i> (sensu Erba)		110.3	10
Aptian/Albian boundary		112.2	
B <i>Prediscosphaera columnata</i> (<5 um)		112.5	10
T <i>Assipetra intracretacea</i>		113.0	10
B <i>Hayesites albiensis</i>		114.0	10
T <i>Micrantholithus hoschulzii</i>		114.2	10
T <i>Nannoconus</i> st. <i>steinmanii</i>		114.2	10
B <i>Braarudosphaera africana</i>		118.2	10
B <i>Stoverius achylosum</i>		118.2	10
B <i>Eprolithus floralis</i>		119.0	10
B <i>Rhagodiscus angustus</i>		119.9	10
T nannoconid paracme		120.5	10

Table T3 (continued).

Event	Zone (Base)	Age (Ma)	Reference
Barremian/Aptian boundary		121.0	
B <i>Rucinolithus irregularis</i>		121.1	10
B <i>Flabellites oblongus</i>		121.1	10

Notes: B = base, T = top. References: 1 = Berggren et al. (1995a); 2 = Sigurdsson, Leckie, Acton, et al. (1997); 3 = Curry, Shackleton, Richter, et al. (1995); 4 = Raffi and Flores, 1995; 5 = Gartner, 1992; 6 = Berggren et al. (1985b); 7 = Backman (1987); 8 = Backman (1986). References 3 through 9 have been calibrated to the time scale of Berggren et al. (1995a, 1995b).

Table T4. Ages of planktonic foraminifer datum levels from Leg 182. (See table notes. Continued on next two pages.)

Event	Zone (base)	Age (Ma)	Reference
T <i>Globorotalia flexuosa</i>		0.07	Joyce et al., 1990
B <i>Bolliella calida</i>		0.22	Chaproniere et al., 1994
T <i>Globoquadrina pseudofoliata</i>		0.22	Chaproniere et al., 1994
B <i>Globorotalia flexuosa</i>		0.40	Joyce et al., 1990
B <i>Globorotalia hirsuta</i>		0.45	Pujol and Duprat, 1983
T <i>Globorotalia tosaensis</i>	Pt1b	0.65	Srinivasan and Sinha, 1992
B <i>Globorotalia crassaformis hessi</i>		0.75	Chaproniere et al., 1994
T <i>Pulleniatina finalis</i>		1.40	Chaproniere et al., 1994
T <i>Globigerinoides fistulosus</i>	Pt1a	1.77	Berggren et al., 1995b
T <i>Globigerinoides extremus</i>		1.77	Berggren et al., 1985b
Pliocene/Pleistocene boundary		1.77	
B <i>Globorotalia truncatulinoides</i>		2.00	Zijderveld et al., 1991
B <i>Globorotalia truncatulinoides</i>	(SN14)		Jenkins, 1993
T <i>Globorotalia exilis</i> (Atl.)		2.15	Berggren et al., 1985b
T <i>Globorotalia miocenica</i>	Pl6	2.30	Berggren et al., 1995b
T <i>Neogloboquadrina atlantica</i>		2.41	Weaver and Clement, 1987
T <i>Globorotalia puncticulata</i> (Atl.)		2.41	Zijderveld et al., 1991
T <i>Globorotalia pertenuis</i>		2.60	Berggren et al., 1985b
T <i>Dentoglobigerina altispira</i>	Pl5	3.09	Berggren et al., 1995b
T <i>Globorotalia multicamerata</i>		3.09	Berggren et al., 1985b
T <i>Sphaeroidinellopsis seminulina</i>	Pl4	3.12	Berggren et al., 1995b
B <i>Sphaeroidinella dehiscens sensu stricto</i>		3.12	Weaver and Clement, 1987
B <i>Globorotalia inflata</i>	(SN13)	(3.20)	Jenkins, 1993; Chaproniere et al., 1995
T <i>Globorotalia</i> sp. cf. <i>G. crassula</i> (N. Atl.)		3.25	Berggren et al., 1985b
B <i>Globorotalia pertenuis</i>		3.33	Berggren et al., 1985b
B <i>Globorotalia miocenica</i> (Atl.)		3.45	Berggren et al., 1985b
T <i>Globorotalia margaritae</i>	Pl3	3.58	Berggren et al., 1995b
T <i>Pulleniatina primalis</i>		3.58	Srinivasan and Sinha, 1992
<i>Pulleniatina</i> trans. sinistral-dextral		3.65	Berggren et al., 1985b
T <i>Pulleniatina spectabilis</i>		3.95	Berggren et al., 1985b
T <i>Globoturborotalita nepenthes</i>	Pl2	4.18	Berggren et al., 1995a
B <i>Globorotalia puncticulata</i>		4.20	Berggren et al., 1985b
B <i>Globorotalia crassaformis</i>		4.50	Weaver and Clement, 1987
T <i>Globigerinoides seiglei</i>		4.50	Chaproniere et al., 1994
T <i>Globorotalia cibaensis</i>	Pl1b	4.60	Berggren et al., 1995b
B <i>Sphaeroidinella dehiscens sensu lato</i>		4.70	Berggren et al., 1985b
B <i>Globorotalia margaritae</i>		5.20	Srinivasan and Sinha, 1992
Miocene/Pliocene		5.25	
T <i>Globorotalia tumida</i>		5.32	Srinivasan and Sinha, 1992
B <i>Globorotalia tumida</i>	Pl1a	5.60	Chaproniere et al., 1994
B <i>Globorotalia sphericomiozea</i>		5.60	Srinivasan and Sinha, 1992
B <i>Globorotalia pliozea</i>		5.60	Srinivasan and Sinha, 1992
B <i>Globorotalia pliozea</i>		5.60	Berggren et al., 1985b
B <i>Globorotalia puncticulata</i>	(SN12)	(5.30)	Jenkins, 1993; Chaproniere et al., 1995
B <i>Globorotalia tumida</i>		5.60	Berggren et al., 1985b
T <i>Globoquadrina dehiscens</i>		5.60	Chaproniere et al., 1994
T <i>Globoquadrina dehiscens</i>		5.80	Berggren et al., 1985b
T <i>Globorotalia linguaensis</i>	M14	6.00	Chaproniere et al., 1994
B <i>Globorotalia margaritae</i>		6.00	Chaproniere et al., 1994
B <i>Neoglob. acostaensis</i> trans. sinistral-dextral		6.00	Chaproniere et al., 1994
B <i>Globorotalia margaritae</i>		6.20	Srinivasan and Sinha, 1992
B <i>Pulleniatina primalis</i>		6.40	Chaproniere et al., 1994
B <i>Globorotalia menardii</i> form 5		6.40	Chaisson and Leckie, 1993
B <i>Neoglob. acostaensis</i> trans. dextral-sinistral		6.40	Srinivasan and Sinha, 1992
B <i>Neoglob. atlantica</i> trans. dextral-sinistral		6.60	Srinivasan and Sinha, 1992
B <i>Globorotalia conomiozea</i>		6.80	Spiegler and Jansen, 1989
B <i>Globorotalia conomiozea</i>	(SN11)	(7.12)	Jenkins, 1993; Chaproniere et al., 1995
B <i>Globorotalia menardii</i> form 5		7.12	Krijgsman et al., 1994
T <i>Globorotalia menardii</i> form 4		7.20	Krijgsman et al., 1994
B <i>Globorotalia suterae</i>		7.40	Krijgsman et al., 1994
B <i>Globorotalia cibaensis</i>		7.80	Glacon et al., 1990
B <i>Globorotalia juanai</i>		7.80	Chaisson and Leckie, 1993
B <i>Candeina nitida</i>		8.10	Chaisson and Leckie, 1993
B <i>Gls. extremus/Glt. plesiotumida</i>	M13b	8.30	Berggren et al., 1995b
T <i>Neogloboquadrina continuosa</i>	(SN10)		Jenkins, 1993
B <i>Neogloboquadrina humerosa</i>		8.50	Berggren et al., 1985b

Table T4 (continued).

Event	Zone (base)	Age (Ma)	Reference
B <i>Neogloboquadrina pachyderma</i>		9.20	Berggren, 1992
T <i>Neogloboquadrina nympha</i>		10.10	Berggren, 1992
T <i>Neogloboquadrina nympha</i>	(SN9)		Jenkins, 1993
B <i>Neogloboquadrina acostaensis</i>	M13	10.90	Berggren et al., 1995b
B <i>Neogloboquadrina acostaensis</i>		10.90	Miller et al., 1991
T <i>Neogloboquadrina mayeri</i>	M12	11.40	Miller et al., 1994
T <i>Neogloboquadrina mayeri</i>	(SN8)		Jenkins, 1993
B <i>Globoturbotalita nepenthes</i>	M11	11.80	Blow, 1979
B <i>Globoturbotalita nepenthes</i>		11.80	Miller et al., 1994
T <i>Globorotalia panda</i>		11.80	Berggren, 1993
T <i>Globorotalia fohsi robusta</i>	M10	11.90	Berggren et al., 1985b
T <i>Globorotalia praescitula</i>		11.90	Berggren, 1992
T <i>Globorotalia fohsi lobata</i>		12.10	Wright and Miller, 1992
B <i>Neogloboquadrina mayeri</i>	(SN7)	(12.10)	Jenkins, 1993; Chaproniere et al., 1995
B <i>Globorotalia fohsi robusta</i>	M9b	12.30	Berggren, 1992
T <i>Tenuitella clemenciae</i>		12.30	Li et al., 1992
T <i>Tenuitella minutissima</i>		12.30	Li et al., 1992
T <i>Tenuitella pseudoedita</i>		12.30	Li et al., 1992
T <i>Tenuitella selleyi</i>		12.30	Li et al., 1992
B <i>Globorotalia fohsi lobata</i>	M9a	12.50	Wright and Miller, 1992
B <i>Globorotalia fohsi sensu stricto</i>	M8	12.70	Wright and Miller, 1992
B <i>Globorotalia praefohsi</i>		12.70	Wright and Miller, 1992
B <i>Neogloboquadrina nympha</i>		13.40	Berggren, 1992
T <i>Globorotalia peripheroronda</i>		14.60	Berggren et al., 1985b
B <i>Globorotalia peripheroacuta</i>	M7	14.80	Berggren et al., 1995a
T <i>Praeorbulina sicana</i>		14.80	Berggren et al., 1985b
T <i>Praeorbulina glomerosa sensu stricto</i>		14.80	Berggren et al., 1985b
B <i>Orbulina suturalis</i>	M6	15.10	Berggren et al., 1985b
B <i>Orbulina suturalis</i>	(SN6)		Jenkins, 1993
T <i>Globorotalia miozea</i>		15.90	Berggren, 1992
B <i>Praeorbulina circularis</i>		16.00	Berggren et al., 1985b
B <i>Praeorbulina glomerosa</i>	M5b	16.10	Berggren et al., 1995a
B <i>Praeorbulina glomerosa</i>	(SN5)		Jenkins, 1993
B <i>Globigerinoides diminutus</i>		16.10	Berggren et al., 1985b
B <i>Praeorbulina curva</i>		16.30	Berggren et al., 1985b
B <i>Praeorbulina sicana</i>	M5	16.40	Berggren et al., 1985b
T <i>Globorotalia incognita</i>		16.40	Berggren, 1992
B <i>Globorotalia birnageae</i>	M4b	16.70	Berggren et al., 1995a
B <i>Globorotalia miozea</i>		16.70	Berggren, 1992
B <i>Globorotalia birnageae</i>		16.70	Berggren et al., 1985b
T <i>Catapsydrax dissimilis</i>	M4	17.30	Berggren et al., 1985b
T <i>Globorotalia zealandica</i>		17.30	Li et al., 1992
T <i>Globorotalia semivera</i>		17.30	Berggren et al., 1985b
T <i>Globoquadrina dehiscens forma spinosa</i>		17.90	Berggren et al., 1985b
B <i>Globorotalia praescitula</i>		18.50	Miller et al., 1994
B <i>Globorotalia insueta</i>	M3	18.80	Berggren et al., 1995a
B <i>Globigerinoides trilobus</i>	(SN4)		Jenkins, 1993
B <i>Globigerinoides altiapertura</i>		20.50	Montanari et al., 1991
B <i>Globoturbotalita connecta</i>	(SN3)	(20.9)	Jenkins, 1993; Chaproniere et al., 1995
T <i>Tenuitella munda</i>		21.40	Li et al., 1992
T <i>Globorotalia kugleri</i>	M2	21.50	Montanari et al., 1991
B <i>Globorotalia incognita</i>		21.60	Berggren, 1992
T <i>Globoturbotalita angulisuturalis</i>		21.60	Berggren et al., 1985b
T <i>Globorotalia pseudokugleri</i>		21.60	Berggren et al., 1985b
B <i>Globoquadrina dehiscens forma spinosa</i>		22.20	Berggren et al., 1985b
B <i>Globoturbotalita woodi</i>	(SN2)	(22.6)	Jenkins, 1993; Chaproniere et al., 1995
T <i>Globoquadrina globularis</i>		22.80	Berggren et al., 1985b
B <i>Globoquadrina dehiscens</i>	M1b	23.20	Berggren et al., 1985a
B <i>Globoquadrina dehiscens</i>	(SN1)		Jenkins, 1993; Chaproniere et al., 1995
B <i>Globorotalia kugleri</i>	M1	23.80	Berggren et al., 1985a
B <i>Globorotalia mendacis</i>		23.80	Berggren et al., 1985a
Oligocene/Miocene boundary		23.80	
T <i>Globigerina euapertura</i>		23.80	Berggren, 1992
T <i>Tenuitella gemma</i>		24.30	Li et al., 1992
FCO <i>Globigerinoides primordius</i>		24.30	Berggren et al., 1985a
B <i>Globorotalia pseudokugleri</i>		25.90	Leckie et al., 1993
B <i>Globigerinoides primordius</i>		26.70	Leckie et al., 1993
T <i>Paragloborotalia opima opima</i>	P22	27.10	Berggren et al., 1985a

Table T4 (continued).

Event	Zone (base)	Age (Ma)	Reference
T <i>Globigerina labiacrassata</i>		27.10	Berggren, 1992
LCO <i>Chiloguembelina cubensis</i>	P21b	28.50	Li et al., 1992
T <i>Chiloguembelina cubensis</i>	(SP15)		Jenkins, 1993
B <i>Globigerina angulisuturalis</i>	P21	28.50	Blow, 1969
B <i>Globigerinita boweni</i>		28.50	Li et al., 1992
B <i>Globigerina angulisuturalis</i>	P21a	29.40	Leckie et al., 1993
B <i>Tenuitellinata juvenilis</i>		29.70	Li et al., 1992
T <i>Subbotina angiporoides</i>		30.00	Berggren, 1992
T <i>Subbotina angiporoides</i>	(SP14)		Jenkins, 1993
T <i>Turborotalia ampliapertura</i>	P20	30.30	Miller et al., 1993
B <i>Paragloborotalia opima opima</i>		30.60	Berggren et al., 1985a
T <i>Subbotina brevis</i>	(SP13)	(31.5)	Jenkins, 1993; Chaproniere et al., 1995
T <i>Pseudohastigerina</i> spp.	P19	32.00	Miller et al., 1993
B <i>Subbotina brevis</i>	(SP12)	(33.4)	Jenkins, 1993; Chaproniere et al., 1995
B <i>Cassigerinella chipolensis</i>		33.65	Miller et al., 1993
Eocene/Oligocene boundary		33.70	
T <i>Hantkenina</i> spp.		33.70	Coccioni et al., 1988
T <i>Turborotalia cerroazulensis</i>	P18	33.80	Coccioni et al., 1988
T <i>Cribohantkenina inflata</i>	P17	34.00	Coccioni et al., 1988
T <i>Globigerapsis index</i>		34.30	Berggren, 1992
B <i>Turborotalia cunialensis</i>	P16	35.20	Coccioni et al., 1988
T <i>Turborotalia pomeroli</i>		35.30	Premoli-Silva et al., 1988
T <i>Porticulasphaera semiinvoluta</i>		35.30	Premoli-Silva et al., 1988
B <i>Cribohantkenina inflata</i>		35.50	Coccioni et al., 1988
T <i>Acarinina</i> spp.		37.50-38.50	Nocchi et al., 1986
T <i>Acarinina aculeata</i>	(SP11)	(36.7)	Jenkins, 1993; Chaproniere et al., 1995
T <i>Acarinina collactea</i>		37.70	Berggren et al., 1985a
T <i>Subbotina linaperta</i>		37.70	Berggren, 1992
T <i>Morozovella spinulosa</i>		38.10	Berggren et al., 198a5
B <i>Porticulasphaera semiinvoluta</i>	P15	38.40	Nocchi et al., 1986
T <i>Planorotalites</i> spp.		38.50	Nocchi et al., 1986
T <i>Acarinina primitiva</i>		39.00	Stott and Kennett, 1990
T <i>Subbotina frontosa</i>		39.30	Berggren et al., 1985a
T <i>Globigerinapsis beckmanni</i>	P14	40.10	Berggren et al., 1985a
B <i>Globigerinapsis beckmanni</i>	P13	40.50	Berggren et al., 1985a
T <i>Acarinina bullbrookii</i>		40.50	Berggren et al., 1985a
B <i>Chiloguembelina cubensis</i>	(SP10)	(41.2)	Jenkins, 1993; Chaproniere et al., 1995
B <i>Turborotalia pomeroli</i>		42.40	Berggren et al., 1985a
B <i>Globigerapsis index</i>		42.90	Berggren et al., 1985a
B <i>Globigerapsis index</i>	(SP9)		Jenkins, 1993
B <i>Morozovella lehneri</i>		43.50	Berggren et al., 1985a
T <i>Morozovella aragonensis</i>	P12	43.60	Berggren et al., 1985a
B <i>Globigerinapsis kugleri</i>	P11	45.80	Berggren et al., 1995a
B <i>Turborotalia possagnoensis</i>		46.00	Berggren et al., 1995a
T <i>Morozovella crater</i>	(SP8)	(48.8)	Jenkins, 1993; Chaproniere et al., 1995
B <i>Hantkenina nutalli</i>	P10	49.00	Berggren et al., 1985a
B <i>Planorotalites palmerae</i>	P9	50.40	Berggren et al., 1985a
T <i>Morozovella formosa</i>	P8	50.80	Berggren, 1969
B <i>Acarinina pentacamerata</i>		50.80	Stott and Kennett, 1990
B <i>Morozovella aragonensis</i>	P7	52.30	Berggren et al., 1995a
T <i>Morozovella marginodentata</i>		52.50	Berggren et al., 1995a
T <i>Morozovella lensiformis</i>		52.70	Berggren et al., 1995a
T <i>Subbotina velascoensis</i>		53.50	Berggren et al., 1995a
T <i>Morozovella aequa</i>		53.60	Berggren et al., 1995a
B <i>M. formosa formosa/M. lensiformis</i>	P6b	54.00	Berggren and Miller, 1988
B <i>Morozovella crater</i>	(SP7)	(54.0)	Jenkins, 1993; Chaproniere et al., 1995
B <i>Morozovella lensiformis</i>		54.00	Berggren et al., 1995a
T <i>Morozovella velascoensis</i>	P6	54.70	Berggren et al., 1995a
Paleocene/Eocene boundary		54.70	

Notes: T = top, B = base, Atl. = Atlantic, N. Atl. = North Atlantic, trans. = transition, LCO = least common occurrence. Citations mainly from Berggren et al. (1995a, 1995b). Parentheses in "Zone" column indicate zones taken from Jenkins (1993). Parentheses in "Age" column indicate dates taken from Chaproniere et al. (1995).

Table T5. Example of a data output file produced by Splicer software.

Core, section, interval (cm)	Depth (mbsf)	Raw GRA density (g/cm ³)	Smoothed GRA density (g/cm ³)	Offset (m)	Depth (mcd)
182-1126B-					
1H-1, 7	0.07	1.78	1.78	0	0.07
1H-1, 11	0.11	1.78	1.78	0	0.11
1H-1, 15	0.15	1.76	1.76	0	0.15
1H-1, 19	0.19	1.79	1.78	0	0.19
1H-1, 23	0.23	1.77	1.78	0	0.23
1H-1, 27	0.27	1.77	1.77	0	0.27
1H-1, 31	0.31	1.78	1.76	0	0.31
1H-1, 35	0.35	1.75	1.75	0	0.35
1H-1, 39	0.39	1.71	1.73	0	0.39
1H-1, 43	0.43	1.72	1.72	0	0.43

Note: GRA = gamma-ray attenuation.

Table T6. The standard deviations for chemical analyses.

Constituent	Method	1 standard deviation
Alkalinity	Titration	<1.5%
Chloride	Titration	<0.4%
Silica	IC	~5%
Phosphate	IC	~5%
Ammonia	IC	~5%
Potassium	IC	<6%
Magnesium	IC	<2%
Calcium	IC	<2%
Sulfate	IC	<4%
Sodium	IC	<5%

Note: IC = ion chromatography.

Table T7. Summary of sampling intervals for all physical properties measurements made during Leg 182.

Measurement	Abbreviation	Sampling interval	Period (s)	Comments
<i>P</i> -wave velocity (MST)	PWL	5 cm	4	Not measured for XCB or RCB cores
Bulk density	GRA	5 cm	4	
Natural gamma	NGR	15 cm	28	
Magnetic susceptibility	MS	5 cm	8	
Thermal conductivity	ThermCon	One per core		Only measured in unconsolidated sediment
Index properties	IP	One per section		Measured at higher frequencies in some intervals so that all lithologies are represented
<i>P</i> -wave velocity (z-direct.)	PWS1	One per section		
<i>P</i> -wave velocity (y-direct.)	PWS2	Two per section		
<i>P</i> -wave velocity (x-direct.)	PWS3	Two per section		Frequency increased to five per section in consolidated sediments
Shear strength		One per section		

Notes: Deviations from normal sampling intervals are described in the right-hand column. MST = multisensor track, PWL = *P*-wave logger, XCB = extended core barrel, RCB = rotary core barrel, GRA = gamma-ray attenuation.

Table T8. Specifications of the logging tools used during Leg 182, grouped into tool strings.

Tool strings	Typical logging speed (m/hr)	Individual tools	Properties measured	Sample interval (cm)	Approximate vertical resolution (cm)	Approximate depth of investigation (cm)
Triple combo (total length = ~32 m)	275	HNGS	Natural gamma ray	15	45	Variable
		APS	Porosity	5 and 15	30	15
		HLDS	Bulk density, PEF	15	38	15
		DITE-SFL	Resistivity	15	200/150/90/60	150/76/38
		TAP	Temperature, acceleration, pressure	One per second Four per second One per second		
FMS/sonic (total length = ~27 m)	275	NGT-C	Natural gamma ray	15	45	46
		GPIT	Tool orientation	1 or 15		
		SDT-C	Sonic velocity	15	110	15-30
GHMT (total length = ~9 m)	550	FMS	Resistivity image	0.25	0.5	15
		NGT-C	Natural gamma ray	15	45	25
WST	Stationary	WST	Sonic travelttime	3000-10000		

Note: See Table T9, p. 71, for explanations of acronyms used to describe tool strings and individual tool names.

Table T9. Logging tool and measurement acronyms, and units of measurement.

Tool	Output	Explanation	Units
HNCS		Hostile environment natural gamma-ray sonde	
	HSGR	Standard (total) gamma ray	API
	HCGR	Computed gamma ray (HSGR-HURA)	API
	HFK	Formation potassium	%
	HTHO	Thorium	ppm
	HURA	Uranium	ppm
NGT-C		Natural gamma-ray spectrometry tool	
	SGR	Standard (total) gamma ray	API
	CGR	Corrected gamma ray (SGR-URAN)	API
	POTA	Potassium	%
	THOR	Thorium	ppm
	URAN	Uranium	ppm
APS		Accelerator porosity sonde	
	APLC	Near array porosity (limestone corrected)	%
	FPLC	Far array porosity (limestone corrected)	%
	SIGF	Neutron capture cross section of the formation (Sf)	cu
	STOF	Computed standoff (tool distance from borehole wall)	in
HLDS		Hostile environment lithodensity sonde	
	RHOB	Bulk density (corrected)	g/cm ³
	PEF	Photoelectric effect	barn/e ⁻
	CALI	Caliper (measure of borehole diameter)	in
	DRHO	Bulk density correction	g/cm ³
DITE-SFL		Phasor dual induction tool - spherically focused log	
	IDPH	Phasor deep induction (deep resistivity)	Ωm
	IMPH	Phasor medium induction (medium resistivity)	Ωm
	SFLU	Spherically focused log uncorrected (shallow resistivity)	Ωm
LDEO-TAP		Temperature/acceleration/pressure tool	
	T, A, P	Temperature, acceleration, pressure	°c, mm/s ² , psi
SDT-C		Sonic digital tool	
	DTCO	Compressional transit time (computed "slowness")	μs/ft
	DT (L, LN, LF)	Transit time (analog "slowness")	μs/ft
	LTT (1-4)	Transit time (long spacing)	μs
	TT (1-4)	Transit time (short spacing)	μs
	ITT	Integrated transit time	s
GPIT		General-purpose inclinometer tool	
	A (X, Y, Z)	Acceleration on X, Y, and Z axis	ft/s ²
	FINC	Inclination	°
	DEVI	Deviation	°
	C1, C2	Caliper 1, Caliper 2 (from FMS tool)	in
	P1AZ	Pad One azimuth	°
GHMT		Geologic high-resolution magnetic tool	
	MAGS	Magnetic susceptibility (limited range)	ppm
	RMGS	Low resolution magnetic susceptibility (wider range)	ppm
WST		Well seismic tool	
	Δt	Acoustic traveltimes	ms

Note: FMS = Formation MicroScanner, API = American Petroleum Institute.

Table T10. Lamont-Doherty Earth Observatory temperature/acceleration/pressure tool specifications (memory mode).

Measurement	Specification
Acceleration measurement range	-2 G to +2 G
Acceleration resolution	1 mm/s ²
Acceleration sampling rate:	
LR mode	4 Hz
HR mode	8 Hz
Temperature measurement range	-4°C to +85°C
Temperature resolution	0.005°C
Pressure measurement range	0 to 10,000 psi
Pressure resolution	1 psi
Pressure measurement precision	0.1% of full scale
Temperature/pressure sampling rate	1 Hz
Total data recording time:	
HR mode	5 hr
LR mode	8 hr
Power source	Eight 1.5-V alkaline batteries (D type)
Total operation time off one set of batteries	~40 hr

Note: LR = low resolution, HR = high resolution.

Table T11. Acquisition parameters for multichannel seismic surveys used to establish the regional seismic stratigraphy in the western Great Australian Bight.

Survey:	ESSO 1979	JNOC 1990	AGSO 1996
Line name prefix:	E79A-	JA90-	S169/
Source:	32 air guns	64 sleeve air guns	3 (6) GI air guns
Volume:	1450 in ³	2180 in ³	450 (900) in ³
Shot interval:	25 m	25 m	12.5 (25) m
Sample rate:	4 ms	4 ms	1 ms
Record length:	6 s	6 s	3.5 (8.5) s
Cable length:	2400 m	3000 m	1000 m
Cable offset:	240 m	200 m	69.9 m
Number of groups:	48	240	80
Group interval:	50 m	12.5 m	12.5 (25) m
CDP interval:	25 m	6.25 m	6.25 (12.5) m
Fold coverage:	48	60	40 (20)

Notes: Survey abbreviations: ESSO = Esso Australia; JNOC = Japan National Oil Corporation; AGSO = Australian Geological Survey Organisation; GI = generator-injector; CDP = common depth point. The parameters applied during deep-water components of AGSO Survey 169 (Lines S169/08 to S169/12) are shown in parentheses.